Resources, Conservation & Recycling 206 (2024) 107643

Contents lists available at ScienceDirect

Resources, Conservation & Recycling

journal homepage: www.sciencedirect.com/journal/resources-conservation-and-recycling

Assessing performance in lithium-ion batteries recycling processes: A quantitative modeling perspective

Marco Vaccari [a,*], Filippo Parlanti [a], Fabio M. Manni [b], Martina Orefice [b], Fabrice Mathieux [b], Gabriele Pannocchia [a], Leonardo Tognotti [a], Antonio Bertei [a]

[a] Department of Civil and Industrial Engineering, University of Pisa, Largo Lazzarino 2, 56122 Pisa, Italy
[b] European Commission – Joint Research Centre, Via E. Fermi 2749, 21027 Ispra, Italy

ARTICLE INFO

Keywords:
Lithium-ion battery recycling
Unit operation
Material recovery
Hydrometallurgy
Pyrometallurgy
End-of-waste

ABSTRACT

In the shift toward sustainable energy solutions, the efficiency of lithium-ion battery (LIB) recycling within the supply chain is of paramount importance. This study evaluates the performance of LIB recycling processes by advancing a quantitative modeling approach. Through process simulations, a comprehensive assessment of pyrometallurgical and hydrometallurgical LIB recycling processes is presented by focusing on the key parameters that influence material recoveries and yields. Recycling efficiency indicators, accounting for the quantity and quality of recycled materials, are introduced and their dependence on the share of different battery chemistries and formats in the spent batteries feed is assessed via numerical simulations. A sensitivity analysis of process parameters identifies the unit operations mostly affecting the recycling performance, highlighting process criticalities. The model presented and its outcomes provide a valuable guide for stakeholders in the LIB industry, aiding informed decision-making to enhance sustainability and resource recovery in the ecosystem of electrochemical energy storage.

List of acronyms

Acronym	Description
ACN	Acetonitrile
BRY	Battery recovery yield
CAM	Cathode active material
CB	Carbon black
CHB	Cyclo-hexyl benzene
CRM	Critical raw material
DMC	Di-methyl-carbonate
EC	Ethylene carbonate
EMC	Ethyl-methyl-carbonate
EOL	End-of-life
EU	European Union
EV	Electric vehicles
LCA	Life cycle assessment
LCO	Lithium cobalt oxide, $LiCoO_2$
LFP	Lithium iron phosphate, $LiFePO_4$
LIB	Lithium-ion battery
LMO	Lithium manganese oxide, $LiMn_2O_4$
MEFA	Material and energy flow analysis
MY	Material yield
NCA	Lithium nickel cobalt aluminum oxide, $LiNi_xCo_yAl_zO_2$
NMC	Lithium nickel manganese cobalt oxide, $LiNi_xMn_yCo_zO_2$
PC	Propylene carbonate
PL	Purity level
PP	Polypropylene
PVDF	Polyvinylidene fluoride
SF	Separation factor
SI	Supplementary information

1. Introduction

In the face of pressing global challenges such as climate change and the depletion of natural resources, the move towards a sustainable and climate-neutral society has become imperative. Strategic initiatives like the European Green Deal (European Commission, 2021a) and Horizon Europe (European Commission, 2021b) plans have placed the European Union (EU) at the forefront of the green transition. A key focus is the decarbonization of the transport sector through the adoption of electric

* Corresponding author.
E-mail address: marco.vaccari@unipi.it (M. Vaccari).

https://doi.org/10.1016/j.resconrec.2024.107643
Received 27 October 2023; Received in revised form 26 March 2024; Accepted 13 April 2024
Available online 25 April 2024

vehicles (EVs), leading to a substantial reduction in greenhouse gas emissions. As EV adoption accelerates, the demand for lithium-ion batteries (LIBs) as the primary technology for electric propulsion and stationary energy storage applications also rises.

However, with the expected lifespan of LIB systems ranging from 10 to 15 years (Masias et al., 2021), a considerable volume of end-of-life (EOL) LIBs is projected to emerge soon. By 2030, it is anticipated that 140 million EVs will globally generate approximately 11 million tons of spent batteries (Thompson et al., 2020). If not properly managed or used in second life applications (Ferrara et al., 2021), these EOL LIBs can pose a significant waste-management challenge (Meshram et al., 2020; Mrozik et al., 2021), but they also present an opportunity for valuable resource recovery through recycling (Harper et al., 2019; Mossali et al., 2020; Or et al., 2020).

LIB recycling is driven by various factors, including environmental concerns, economic incentives, and the need to save exploitation of critical raw materials (CRMs) such as lithium, cobalt, nickel, manganese, and natural graphite (Baars et al., 2021; European Commission, 2023). The European Commission's focus on CRMs underscores the importance of recycling in establishing a closed-loop supply chain for these essential materials (Bobba et al., 2020; Yang et al., 2023). Nevertheless, recycling LIBs is a complex task due to their lack of standardization in cathode chemistries, geometries, and sizes, necessitating innovative and adaptable recycling processes (Windisch-Kern et al., 2022). Several LIB recycling routes have been proposed and implemented, with pyrometallurgy-based processes being the most established in EU, followed by hydrometallurgy-based and co-precipitation routes (Latini et al., 2022; Makuza et al., 2021; Sommerville et al., 2021). Additionally, there is a growing interest in the development of a direct recycling route, which aims to regenerate cathode and anode active materials by using non-destructive methods (Larouche et al., 2020; Wu et al., 2023; Xu et al., 2020; Zhang et al., 2023). As the recycling landscape evolves, the pursuit of "greener" technologies is also gaining traction at the research level (Cattaneoet al., 2023; Jegan Roy et al., 2022; Leal et al., 2023; Morina et al., 2022).

A recent review paper provided a systematic and updated analysis and classification of LIB recycling processes, aiming to complement previous studies on legislative considerations, environmental impacts, and future perspectives (Latini et al., 2022). This extensive survey of industrial and pilot recycling processes allowed for the characterization, classification, and comparison of unit operations, critical aspects, and industrial readiness. By analyzing recycling processes in terms of the quality of recycled outputs, this work revealed that a quantitative analysis of such processes is needed to fully contribute to the development of harmonized rules for evaluating recycling indicators and informing policy and industrial decision-makers.

Modeling and simulation are two pillars at the base of performing quantitative assessments on different aspects of the LIB value chains including modeling of specific unit operations (Lu et al., 2021; Punt et al., 2023; Yuan et al., 2023), techno-economic (Lander et al., 2021; Maisel et al., 2023; Thompson et al., 2021; Yang et al., 2021) or life cycle assessments (LCA) (Arshad et al., 2022; Tao et al., 2023; Yu et al., 2021). Modeling can also give guidelines to the design of new LIBs with recycled cathode active material (CAM) assessing their potential electrochemical limitations (Lagnoni et al., 2022).

In the literature, the long-term economic and environmental impacts of recycling LIBs within the supply chain network have been evaluated in a hybrid analysis which adopted an approach that combined agent-based, system dynamics, and metallurgical process analyses considering waste collection, transportation, and recycling plant operations (Wasesa et al., 2022). Exploring scenarios with different LIB waste types and collection rates, the study emphasized the importance of cost-benefit analysis when selecting the appropriate LIB recycling process, as its feasibility depends on factors like LIB waste composition, operating costs, energy consumption, and waste outputs. On the other hand, Blömeke et al. (2022) developed a material and energy flow analysis on the process unit level based on physical and chemical relationships to assess the environmental and economic impacts of three widely used LIB recycling routes. The analysis focused on pyrometallurgical, mechanical, and thermal-mechanical pretreatments, and subsequent hydrometallurgical material recovery, revealing how mechanical pretreatment followed by hydrometallurgy has the best trade-off (high economic benefit and low environmental impacts) while the pyrometallurgical pretreatment produces large amounts of slag, that need to be processed hydrometallurgically, thus incrementing the environmental impacts. A similar approach, which proposes a LCA based on material and energy flows data quantified via a flowsheet simulation, was presented by Rinne et al. (2021), albeit limited to hydrometallurgical recycling only.

Clearly, achieving a sustainable circular economy for LIBs requires a combination of supply chain management, sustainability assessment, and process engineering (Fan et al., 2020; Lin et al., 2023). However, quantifying advancement potentials can be challenging due to interdependencies between recycling processes and resulting product qualities. To address this, combining physical models with environmental and economic assessments can offer a quantifiable approach. Additionally, studying how product design influences recycling becomes crucial (Neumann et al., 2022), especially when the battery producer is also involved in utilizing recycled materials to produce new batteries (Lagnoni et al., 2022). In other words, a clear analysis of how the performance of such recycling routes depends on different technical factors is still to be addressed.

This study introduces an advanced simulation model, operating at the process unit level, and extends methodologies like the material and energy flow analysis (MEFA) employed in previous studies (see Blömeke et al., 2022 and references therein). The model dynamically assesses how the performance of pyrometallurgical and hydrometallurgical recycling routes responds to shifts in LIB input flows, alterations in operational conditions, and changes in yield requirements. In the ever-evolving landscape of LIB recycling, the versatility of the model makes it a powerful asset, serving stakeholders across multiple tiers with distinct needs and goals in a forward-looking approach. The model numerically evaluates the impact of different chemistries of LIBs entering the recycling routes, offering critical insights for industries adapting to diverse feedstock compositions. In addition, the model adaptability to different future scenarios, including variations in the share of large and small format LIBs, enables for a quantitative assessment of the influence of these variations on recycling indicators. A robustness analysis is introduced to reveal the most sensitive unit operations within each process: this capability is essential for understanding how changes in operational parameters can significantly impact recycling indicators, guiding decision-makers towards optimizing specific steps for overall recycling performance enhancement. Researchers can leverage its capabilities to delve into specific subject areas, contributing to the refinement and innovation of LIB recycling methodologies. On the other hand, the tool's inherent capacity enables comprehensive analyses of the burgeoning EU LIBs recycling infrastructure. By scrutinizing performance metrics, identifying bottlenecks, and uncovering optimization opportunities, this tool empowers stakeholders to navigate the intricate landscape of LIB recycling with informed strategies.

The study is organized as follows. First, a description of the proposed modeling is given in Section 2 illustrating its framework (Section2.1) and the two modeled recycling routes: a pyrometallurgy-based process (Section2.2) and a hydrometallurgy-based one (Section2.3). A detailed lists of parameters and data used for the modeling can be found in the Supplementary Information (SI). Then, LIB recycling routes are quantitatively analyzed in detail in Section 3, first introducing the performance indicators and the main assumptions adopted (Section 3.1) and then performing a robustness analysis testing different spent LIBs inputs (Section 3.2). Section 3.3 then evidences the most sensitive operations in each recycling route. A final discussion of implications and possible

future directions of the presented model are reported in Section 4.

2. Model description

2.1. Generalities

In this section, the basic functioning and characteristics of the developed model are described to explain its rationale and potentiality.

Among the different LIBs recycling routes available at the industrial and pilot level (Latini et al., 2022), the proposed model simulates two representative routes.

The first one is the Umicore–Valéas pyrometallurgical process based on recovering an alloy of valuable metals, such as Ni, Co, and Cu, by smelting the entire battery. While these materials can then be subsequently treated to obtain individual metal salts with a high degree of purity, plastic and graphite contained within the cells are inevitably burnt. Furthermore, Li, Al, Mn, and Fe mainly end-up in the slag (Windisch-Kern et al., 2022).

The second process modeled is representative of the hydrometallurgical route, more specifically the process chosen is the LithoRec one and its co-precipitation route (Kwade and Diekmann, 2018). This is an alternative process that can be seen as a hydrometallurgy-based route which promotes a closed-loop on CAM. In this method, the black mass obtained via mechanical pretreatments is firstly leached and the impurities removed; then, the cathode precursors are simultaneously co-precipitated as a hydroxide, and subsequently sintered into the CAM. Therefore, after an initial rupture of its crystal structure, the CAM is re-synthesized to be reused to produce LIBs.

In addition to being two processes relevant to represent the LIB recycling spectrum at various technological readiness levels, there is sufficient literature data for simulating these two processes; in fact, reliable process data are essential for a meaningful modeling approach, hence their availability is crucial. About process maturity, the selected pyrometallurgical process is currently one of the most industrially widespread and established method, with different patents and reports (Cheret and Santen, 2007). On the other hand, the second process, extensively detailed in the LithoRec project (Kwade and Diekmann, 2018), emerges as one of the main technologies for material recovery. Currently, only the mechanical separations proposed in the LithoRec project are industrially developed by Duesenfeld (albeit with some modifications), while the co-precipitation steps as described in the LithoRec project are not operational. Nonetheless, these latter steps exhibit similarities to the hydrometallurgical/co-precipitation section conducted by Ascend Elements, warranting their inclusion in this study (Latini et al., 2022).

The two modeled flowcharts of unit operations are directly adapted from Latini et al. (2022), which in turn is derived from the sequence of operations outlined in Kwade and Diekmann (2018).

The proposed modeling framework is depicted in Fig. 1 and structured as follows. The two process models are built in Python using the "class" structure, that is, each unit operation is included within the corresponding class. The input of the code is specified by the input mass of spent LIBs entering the recycling process. Furthermore, a limited number of options allows for a more detailed input specification. This includes indicating the proportion of battery systems (i.e., large vs small format LIBs) in the input feed, along with specifying the distribution of various chemistries present in both large and small format LIBs (i.e., lithium nickel manganese cobalt oxide $LiNi_xMn_yCo_{1-x-y}O_2$, NMC, lithium iron phosphate $LiFePO_4$, LFP, lithium cobalt oxide $LiCoO_2$, LCO, lithium nickel cobalt aluminum oxide $LiNi_xCo_yAl_{1-x-y}O_2$, NCA, and lithium manganese oxide $LiMn_2O_4$, LMO). Clearly, when accurate composition data of small and large format LIBs are available, the basic chemistries considered can be updated. The reference input feed consists of 200 kg of spent LIBs. Concerning the calculation of battery composition, 18,650 format cylindrical batteries are considered as representative of small format LIBs, whereas prismatic LIBs with 50 Ah capacity are representative of LIBs inside EVs battery packs.

The simulation model calculates the propagation, transformation, consumption, and formation, of each material contained in the input spent LIBs throughout the unit operations of the selected process (Umicore or LithoRec). Table 1 reports the list of materials, classified for different parts of the LIB (pack, module, casing, cell), contained in the input spent batteries vector described in the code.

The code is designed to evaluate material and energy balances along the whole recycling route simulated, giving in output the material streams of the material components resulting from various operations.

Within the code, each unit operation of the processes is reproduced according to one of three different approaches, based on how the outputs are calculated from the inputs, as depicted in Fig. 2. The first approach is a "first-principle" approach based on balance equations and physical/chemical constraints applied to each unit operation. In practice, the flowrate and composition of the streams exiting from the unit operation is calculated based on the streams and utilities entering the unit operation according to mass and energy balances, accounting for thermodynamic equilibria (e.g., solubility constants, acid-base equilibria, etc.) and process kinetics (e.g., crystal growth rate, reaction

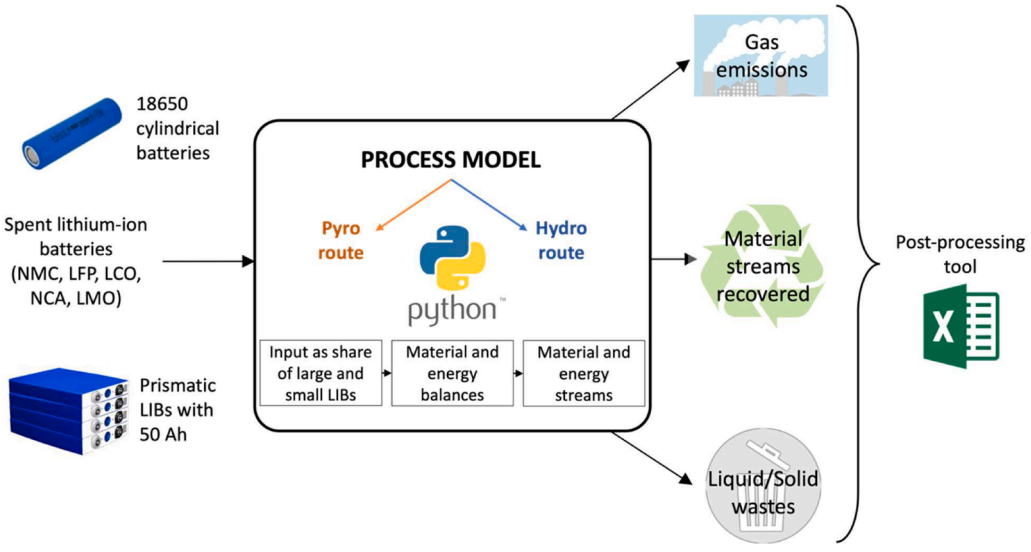

Fig. 1. Conceptual diagram of the proposed modeling framework, evidencing the inputs and the outputs of such structure and the flow of information.

Table 1
List of materials contained in the input vector of the spent LIBs entering the processes. The differentiation into LIBs parts applies only when describing the inputs in the code; in fact, upon entering the process, the distinction between aluminum, plastics, and steel coming from different LIBs parts is no longer adopted.

LIBs part	Materials		LIBs part	Materials			
Pack	Steel	Battery system periphery	Cell	Al foil	Cathode current collector	O	Oxygen in oxidized compounds
	Electronics and Cables	Battery management system and circuit boards		Cu foil	Anode current collector	PP	Separator
				Graphite	Anode	PVDF	Binder for current collectors
	Al	Battery system periphery		Li	Cathode (NMC/NCA/LCO/ LFP)	EC	Organic carbonates in the electrolyte
	Plastics	Connection and isolation		Co	Cathode (NMC/NCA/LCO)	CHB	
Module	Al	Thermal management system		Mn	Cathode (NMC/LMO)	DMC	
	Plastics	Isolation		Ni	Cathode (NMC/NCA)	EMC	
	Steel	Module periphery		Al	Cathode (NCA)	$LiPF_6$	Conductive salt in the electrolyte
Casing	Al	Cell housing		Fe	Cathode (LFP)	CB	Additive to improve electric conductivity
	Steel	Cell housing		P	Cathode (LFP)		

CB: Carbon Black, CHB: Cyclohexylbenzene, DMC: Dimethyl carbonate, EC: Ethylene carbonate, EMC: Ethyl methyl carbonate, PP: Polypropylene, PVDF: Polyvinylidene fluoride

CB: Carbon Black, CHB: Cyclohexylbenzene, DMC: Dimethyl carbonate, EC: Ethylene carbonate, EMC: Ethyl methyl carbonate, PP: Polypropylene, PVDF: Polyvinylidene fluoride.

kinetics, sieving and precipitation rates, etc.). The units solved by first-principles are reported with blue-colored boxes in Fig. 2. This is the case of the hydrometallurgical steps in both modeled processes, for which solubility equilibria and/or main reaction mechanisms are well-established. The second approach follows an opposite strategy: when the physics and chemistry of a unit operation are too complex, or poorly known in the literature, to be described by detailed mechanistic modeling, a "black box" approach is considered; such an approach is also adopted when the unit operation performs a simple splitting of materials, so that a black box approach suffices. Following this strategy, within the code, all the materials that enter a unit operation are redirected to the exiting streams following separation factors (SFs), quantifying the fraction of a material in a specific output stream. As an example, separation factors are used in the "Manual sorting" step in Fig. 2a to quantify the fraction of Al entering such a unit and ending up in the "More valuable fractions" stream, while the remainder is addressed to the "Less valuable fraction" streams. The unit operations described as a black box inherently satisfy mass balances since they represent a simple linear split of materials. These units are reported with grey-colored boxes in Fig. 2, which is the case for most of the mechanical operations. Lastly, a hybrid approach (denoted with blue-grey striped boxes in Fig. 2) is adopted by combining the two previously mentioned methods to describe the operations which require an intermediate level of refinement (e.g., smelting of spent LIBs, leaching of the black mass); in other words, separation factors are adopted along with basic first-principle constraints, such as a stoichiometry check. The selection of modeling approaches for each unit in this study is based on a combination of criteria, including the level of sophistication necessary to model a unit operation given how it impacts the whole process results, as well as the availability and quality of data related to its operating conditions. Furthermore, our modeling approach primarily focus on material flow analysis rather than an in-depth examination of the chemical reactions. The aim is to provide insights into waste material flows and to provide stakeholders with informed findings based on a more granular approach, surpassing the aggregated block diagrams commonly found in the literature (e.g., Blömeke et al., 2022) without entering into detailed evaluations of individual process unit conditions (e.g., Cheng et al., 2019).

To ensure the accuracy and reliability of the simulations, the models have been built using data from different sources. Whenever possible, information is sourced from the literature (scientific papers, open industrial reports, or patents); otherwise, assumptions are made based on expertise.

Upon successfully inputting the desired process parameters into the Python code and running the simulation, a Microsoft Excel file is automatically generated. This file provides detailed information about the material streams entering and leaving the system boundaries and each unit operation, including their flow rate and composition. The Python-

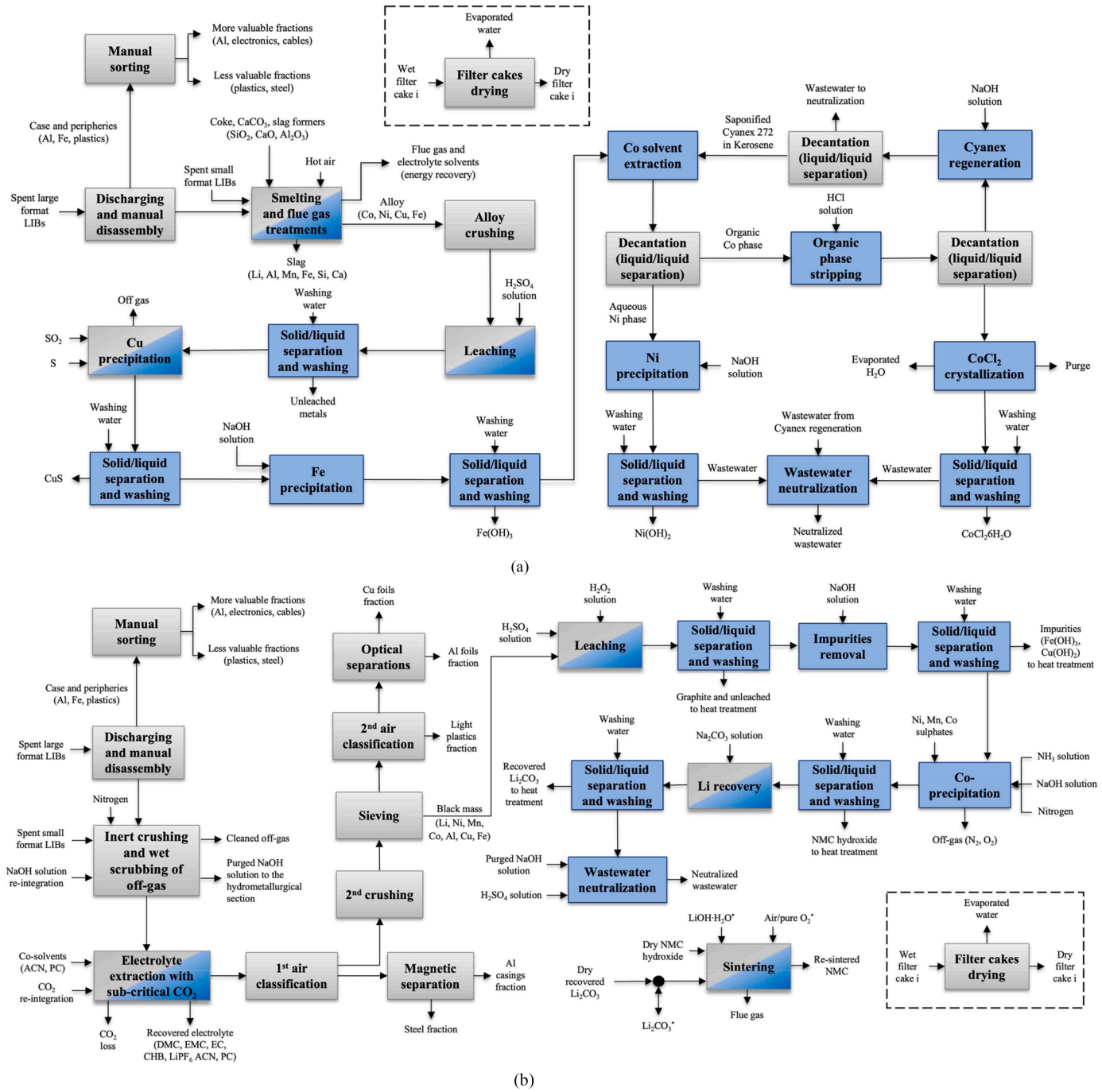

Fig. 2. Block diagrams of the (a) Umicore and (b) LithoRec processes evidencing the modeling approach used for simulating each operation: grey boxes are treated as black box models with SFs, blue ones are described by first-principle models, while the striped ones are a combination of the previous two (adapted from Latini et al. (2022), Kwade and Diekmann (2018)).

Excel integration is also useful to facilitate the calculation of various performance indicators for LIBs recycling processes. As a matter of fact, by performing a post-processing analysis on the material streams obtained from the process simulations conducted using the Python code, different performance metrics can be accurately determined and tested. These performance indicators can play a crucial role in evaluating the effectiveness and efficiency of LIB recycling processes as shown in Section 3.

For a better understanding of how the two chosen processes have been modeled, a more in-depth description of both is given in the next sections, while a complete list of the parameters adopted, and the sources considered for the modeling framework are reported in Tables S1 and S2 of the SI.

2.2. *Umicore–Valéas process*

The simulated Umicore-Valéas process, depicted in Fig. 2a, starts with the discharge of the input spent batteries. This is followed by the disassembly operation where the spent battery systems are manually separated to recover the casing, cables and electronic components, and other peripheral components. To simulate this operation in the Python code, separation factors (SF_{dis}), which represent the recovered mass fraction of each material in the stream, are used. The separated stream is sent to a manual sorting step where operators manually sort the higher

value components (Al and Electronics & Cables) from the lower value components (Fe and Plastics).

The remaining battery material stream coming out of the disassembly is sent to the smelting stage. In this furnace both the evaporated electrolyte and the melted plastic components and binders of the cells burn, while the remaining battery components are transformed into a slag fraction (Li, Al, Si, Mn, Fe in an oxidized state) along with an alloy (Cu, Co, Ni, and Fe in a reduced state). The core of the smelting process is modeled as a black box in which the material flow of auxiliary reactants is calculated by setting their ratio with respect to the flow of disassembled spent LIBs entering the smelter; their default values are taken from Umicore patent (Cheret and Santen, 2007). The ratio between the volumetric airflow of hot oxygen-enriched air and the mass flow of disassembled spent LIBs is another parameter that can be tuned. This must guarantee at least the oxygen amount needed to oxidize the metals included in the slag and for the combustion of the carbon that does not act as reducing agent. To simplify the calculations, SFs (SF_{sme}) are used in the code as parameters which account for the mass fraction of the material fed to the smelter that is recovered in the alloy. Metals in the alloy are assumed to be in the reduced metallic form, whereas the ones within the slag are in their most stable oxide form. In addition, the reducing effect of Al and Cu, present in the feed in their metallic form, is not accounted for, whereas the effect of carbon is considered. In principle, the addition rate of auxiliary reactants should change if the feed contains spent LIBs with steel or with aluminum cell housing, where the latter acts as reducing agent (Latini et al., 2022). The model implementation reflects the conservative conditions in which the large spent LIBs treated are always considered with steel casings. The smelter model does not explicitly consider combustion, pyrolysis or decomposition reactions of organic compounds and electrolyte; thus, these compounds virtually end up in the flue gas in the same form as they enter the smelter. This simplification can still be accepted if the purpose of the model is to evaluate recycling performance indexes and it is not important in which form a material is dispersed in gas emissions. Not only electrolyte organic solvents, PVDF binder and plastics, but also the electrolyte conductive salt $LiPF_6$ is lost in the flue gas in the same form as it enters the smelter. In the proposed modeling approach, the loss of $LiPF_6$ is allocated to the Li lost in the flue gas as fly ash. As a matter of fact, the remainder amount of Li in the battery system is directed into the slag. It is important to note that these simplifications are employed solely for conservative evaluation purposes to assess the fate of Li in the smelter. The actual behavior of Li in the smelting environment involves complex chemical reactions and transformations, which are currently being investigated in the literature to improve its recovery. Indeed, the current research trends involve shifting the proportion of Li in the flue gas rather than the slag to enhance recovery efficiency (Qu et al., 2022). Concerning the energy balance, since modeling of the physical and chemical events in the smelter is extremely complex, a secondary parameter representing the average heat requirement is used to estimate the power consumed by the smelter together with the undisclosed flue gas treatment section. It is defined as the ratio of the required power and the mass flow of spent disassembled LIBs incoming to the smelter (MJ/kg); its value is taken from the literature (Sonoc et al., 2015). Nonetheless, it shall be noted that the smelting unit is modeled with a mixed approach as represented in Figure 2a; this is because the slag composition is governed by oxidation reactions that depend on the oxygen balance within the smelter. As a matter of fact, if no sufficient oxygen in the air flow is supplied to the smelter, the compounds oxidation and the consequent slag formation cannot be achieved, which is a criterion checked within the model.

After crushing, the alloy scraps, containing critical and valuable raw materials, are leached using an inorganic acid solution of H_2SO_4 in an isothermal stirred tank. To simulate the leaching of metals as Fe, Cu, Ni, and Co, leaching SFs (SF_{leach}) on a molar basis are implemented in the model. They represent the amount of metal leached in solution divided by the total amount of that metal in the alloy. Leaching SFs of Ni and Co and operating conditions are taken from Zhang et al. (2018); the remaining leaching SFs for Fe, Al, and Cu are supposed to be 99 % in a conservative way as they are considered impurities to be removed. The leaching reactions are reported in Eq. (S1) of the SI. Given the chemical nature of this unit operation, it necessitates the execution of mass balances for the reactants. Additionally, an estimation of pH is conducted, as this parameter holds significance in subsequent process steps.

At this point, the aqueous solution contains metal ions, which are individually recovered by selective precipitation steps. Cu is removed from the solution as CuS, using concentrated SO_2 and addition of elemental sulfur in an inert gas flow (N_2) (Herrmann et al., 2018). The SF for Cu, representing its precipitation percentage as CuS, is fixed (SF_{pre}^{Cu} = 99 %) (Hong et al., 2020), thus determining the stoichiometric quantity of SO_2 and sulfur needed for the reaction. On the other hand, information on the real industrial-scale or lab-scale operative conditions of the Cu precipitation step could not be found; thus, temperature, pressure, and concentration of SO_2 gas flow are chosen to minimize the gas flow since large gas volumes (i.e., gas/liquid volume ratio greater than 1) can cause problems to impellers in industrial stirred tanks for gas-liquid mixing. As in the previous step, mass balances on the reactants, pH estimation linked to the H_2SO_4 produced in the reaction and energy balances are simulated and performed, considering low-pressure steam to keep the temperature at the fixed value.

In addition, it is important to note that our process modeling presents one approach among many for removing copper, with potential variations from current practices. Therefore, our model should also be interpreted in the context of the broader range of methods available for copper removal, e.g. employing Na_2S to precipitate CuS (Wang et al., 2023).

The precipitation of Fe as a hydroxide is modeled in a different way: instead of being a calculated quantity, the solution pH is used here as an input parameter to regulate Fe precipitation. The selection of operative pH of the Fe precipitation step follows this rationale: first, it should be higher than 4 to remove all the Fe ions, but lower than 7 to limit Ni and Co precipitation, and between 4.5 and 6.5 to optimize the solvent extraction in the following step. The resulting solution containing mainly Co and Ni is pumped into a mixer-settler, where an organic extractant such as Cyanex 272 saponified in kerosene is mixed to separate Co, which dissolves in the organic phase, from Ni, which remains in the aqueous phase. A function of metal extraction efficiency depending on pH and saponified fraction is interpolated from data (Kang et al., 2010). Then, organic and aqueous phases are separated through a decantation based on density difference. The organic phase is fed to a "stripping" tank where a HCl solution is fed to obtain a pH of 2.5, which allows the separation of Co (Flett, 2005). At this point, a further decantation separates the remaining Cyanex 272 dissolved in kerosene from the aqueous solution containing $CoCl_2$. The organic stream is regenerated with NaOH to reach the right saponification condition to be recirculated to the process and undergoes another decantation to separate the aqueous phase, which is sent to wastewater treatment. Instead, the stripped aqueous solution rich in Co is fed to another section where $CoCl_2 \bullet 6H_2O$ is crystallized. This step is carried out in a continuous way using an adiabatic concentrator, operating under vacuum, and an evaporative crystallizer. The mother liquor is recirculated and mixed with the fresh input, after purging a fraction of it to avoid the accumulation and following crystallization of $NiCl_2$ (present as impurity). The main parameters of this block used in the code are the operative temperature of the concentrator and the crystallizer (T_{cry}), the concentration of the solution after the concentrator, and the humidity of the crystal after the solid-liquid separation through the spin dryer (H_{cry}). These parameters are carefully selected after a basic design of the section, which includes the crystallization step, the previous concentration step, and a spin dryer that operates the solid-liquid separation after the crystallization, according to the principles of selection and design of industrial crystallizers (Kramer and Lakerveld, 2019). The crystallizer

and concentrator are adiabatic, while the feed temperature is assumed to be at room temperature, coming from an intermediate storage. The main parameters of the block cannot be varied singularly but must be selected to guarantee the oversaturation of $CoCl_2$ in the crystallizer and, possibly, to avoid the precipitation of $NiCl_2$. The solubility curves of $CoCl_2$ and $NiCl_2$ are interpolated as a function of literature data (Green and Southard, 2019). Coming back to the decantation following Co solvent extraction, the Ni-rich aqueous solution from the first decantation tank is sent to the metal recovery section. Ni is recovered from the aqueous solution via precipitation as $Ni(OH)_2$ via addition of NaOH solution. Nickel hydroxide precipitates along with additional hydroxides coming from impurities in the aqueous solution such as $Fe(OH)_2$, $Co(OH)_2$, and $Cu(OH)_2$.

leached mass fractions of the components. Leaching data for Ni, Mn, and Co are taken from Gratz et al. (2014) while the leaching SF of Li is conservatively supposed to be equal to the lowest one among the previously mentioned metals, whereas leaching SFs of Fe, Al, Cu, and P are supposed to be 99 %. It must be noted that this setting represents a conservative condition since such elements are impurities in the developed hydrometallurgical process. In addition, for Fe and Al, leaching SFs do not consider from which battery parts these metals originate from, be it the cathodic material (e.g., LFP for Fe, NCA for Al), the cell (e.g., Al from collector foils) or the casing (e.g., steel or aluminum cell housing). The leaching reaction of CAM is considered with a unitary conversion according to the reaction scheme reported in Eq. (1).

$$\mathrm{LiNi_{\alpha}Mn_{\beta}Co_{1-\alpha-\beta}O_{2(s)}} + b\mathrm{H_2SO_{4(aq)}} + c\mathrm{H_2O_{2(aq)}} \rightarrow d\mathrm{Li_2SO_{4(aq)}} + e\mathrm{NiSO_{4(aq)}} + f\mathrm{MnSO_{4(aq)}} + g\mathrm{CoSO_{4(aq)}} + h\mathrm{O_{2(g)}} + j\mathrm{H_2O_{(l)}} + \mathrm{Li_{a0}Ni_{b0}Mn_{c0}Co_{d0}O_{e0}} \quad (1)$$

2.3. LithoRec process

The LithoRec process (Fig. 2b) starts with the discharging, manual disassembly, and manual sorting steps of the spent LIBs, which are modeled with the same approach described in the previous section.

After manual disassembly, the battery modules are crushed under inert atmosphere, then the shredded fragments are sieved by the discharge screen and transported to the dryer by the screw conveyor. The exhaust gases from the crusher and dryer are cleaned by a condenser and a wet scrubber, which allow the recovery of the solvents and the removal of toxic HF, respectively. Information and experimental data about these steps are taken from Hanisch et al. (2015).

The shredded fragments undergo a dynamic extraction step of the electrolyte with sub-critical CO_2 to recover both organic solvents and conductive salts, leaving the crushed fragments completely dried. In addition to CO_2, acetonitrile and propylene carbonate are also used as co-solvents (Grützke et al., 2015). This step is implemented by using overall extraction and polar compound extraction separation factors (SF_{el_extr}). To estimate the energy consumption related to this operation, the CO_2 loss and re-integration due to unwanted condensation after lamination, the experimental set-up has been simulated with a closed-loop cycle implemented in UniSim Design®.

Other mechanical separations are operated to obtain the black mass and remove lighter components. First, the dried battery fragments are fed to the first air zigzag sifter, which separates the light fraction (cathodic and anodic active materials, foils, and plastic separator) from the heavy one. The heavy fraction is fed into the subsequent stage of magnetic separation to recover iron. Using a cutting mill, the light fraction fragments are homogenized. Afterwards, the coating active materials of the electrodes are separated using a vibration sieve. The resulting powder is also known as black mass. In the code, this operation is implemented using sieving SFs (SF_{siev}) on a mass basis, which represent the amount of material that goes into the black mass.

Via a second air classification process using zigzag sifting, the other fragments are divided into two fractions: current collector foils (heavy fraction) and plastic separator (light fraction). In the code this step is implemented by means of SFs (SF_{air2}) defined as mass fractions of any compound in the incoming stream that is separated in the heavy fraction. Finally, through optical separations, the current collector foils are divided into a more valuable Cu fraction, which requires high purity, and an Al fraction. All these steps are modeled as black box with SFs taken from Hanisch et al. (2015).

The black mass is directed to a stirred tank in which the leaching reactions take place by adding H_2SO_4 and H_2O_2. The model implementation uses leaching SFs (SF_{leach}) of the materials defined as the

The stoichiometric coefficients *d,e,f,* and *g* are calculated based on the leaching SFs of Li, Ni, Mn, and Co along with coefficients *b* and *c*, for H_2SO_4 and H_2O_2, respectively. The chemical composition of the unleached material (a_0, b_0, c_0, d_0) depends on the selected leaching SFs as well as on the electrical neutrality constraint (e_0). Lastly, coefficients *h* and *j* are determined to fulfil the global molar balance. Reactants concentrations and their excess are main parameters of this unit, and the default values are taken from Gratz et al. (2014) assuming an ideal scale up from lab to industrial scale.

The leachate is sent to another stirred tank together with washing solution and pH is adjusted to have optimal conditions for precipitation of impurities such as $Al(OH)_3$, $Cu(OH)_2$, and $Fe(OH)_3$. In the model, the mass flow of NaOH to be added is calculated to reach the set value of pH considering the precipitation reactions, which are governed by solubility products for the hydroxides whose values are taken from scientific literature. It is to be underlined that the requirements for re-making NMC cathode materials are very stringent regarding the level of impurities (ppm level) contained in the NMC hydroxide. Therefore, often chemical precipitation followed by solvent extraction is needed for effective and economical removal of impurities for producing Ni/Co sulfates that become the raw material for making NMC precursors (the interested reader can see e.g. Davis and Demopoulos, 2023). Nevertheless, it is worth mentioning that, even though this step is referred to simply as “Impurity Removal”, it can encompass multiple unit operations which are often implied.

In each washing section the main parameter is “*humidity*”, defined as the mass ratio between the liquid solution and the dry solid in the filter cake. This parameter, which differs for each washing section, is set so that the liquid in the filter cake soaks the voids created among solid particles. In a conservative way the void fraction of the filter cake is supposed to be equal to 0.36 (Rolland et al., 2019), which refers to a dense random packing of spherical rigid particles. In addition, the amount of washing water fed to such units is supposed to be twice the amount of solution trapped in the filter cake.

After this step, the co-precipitation operation takes place. In this process the aim is to obtain cathode precursors of NMC-111 to be sintered, hence the pH is constantly kept at fixed value and Ni, Mn and Co sulphates are added to achieve both the correct stoichiometry and bulk concentration. The co-precipitation step is the core of the developed hydrometallurgical process and information about this unit operation are taken from Barai et al. (2019). The main parameters used to model this step are the concentration of NH_3 stream used as chelating agent, the concentration of NMC metals in solution, the concentration of NH_3 aqueous solution (in mol NH_4OH/m^3), and the ratio between the N_2 gas flow bubbled in the stirred tank and the liquid volume inside it. In this

study the cathode precursor of NMC-111 is targeted; nevertheless, also other stoichiometries for the NMC product can be handled by the model (i.e. $LiNi_{\alpha}Mn_{\beta}Co_{1-\alpha-\beta}O_2$ for NMC-532, NMC-622, and NMC-811). In any case Ni, Mn, and Co virgin hydrated sulphates have to be added to reach the desired molar ratio (α, β) and, in some cases, also the concentration of NMC metals in solution required for co-precipitation. The operation is assumed to take place at constant pH. This parameter is crucial to maintain the optimal co-precipitation conditions, therefore a proper value of the bulk concentration of NH_3 must be determined to maintain the pH of the resulting mixed solution within the range 11–12 (Vaccari et al., 2023). As a side note, for any value of pH it is assumed that no LiOH precipitates.

On the other hand, leaching of LFP active material releases phosphate ions which, according to typical pH values during leaching and acid/base equilibria, are present in solution as H_3PO_4 and $H_2PO_4^-$; at pH around 7 the equilibrium moves towards $H_2PO_4^-$ and HPO_4^{2-}, whereas PO_4^{3-} ions are present in not negligible concentration only at alkali pH around 12. Co, Ni, Cu, and Mn phosphates are highly insoluble, so they will precipitate in the co-precipitation step causing metal losses and producing impurities in the ternary NMC precursor; that is why LFP batteries should be limited as much as possible in the feed of processes based on co-precipitation method (Kwade and Diekmann, 2018). Also, metal hydrogen phosphates are not much soluble, and some Co, Ni, and Mn might precipitate in this form in the first step after leaching, producing a neutralization or even a pH rise up to ca. 7. Thus, also in typical hydrometallurgical processes, which do not perform co-precipitation, LFP might create valuable metal losses, although this is less critical than the requirements set for co-precipitation, thus allowing a higher share of LFP in process feed. Modeling of all the equilibria of H_3PO_4 is performed via the acid dissociation constants pK_i as shown in Eq. (S3) of the SI. Lastly, it is assumed that all the PO_4^{3-} ions react with Co ions due to the low value of the solubility constant of $Co_3(PO_4)_2$, i.e., $Kps_{Co_3(PO_4)_2} = 10^{-35}$. Hence, when the process handles LFP batteries, $Co_3(PO_4)_2$ might precipitate representing an unacceptable loss of Co which also creates impurities in the NMC precursor.

The solution after co-precipitation contains Li ions, which are precipitated as Li_2CO_3 with a saturated solution of Na_2CO_3 in another stirred tank operated at 50 °C to ensure no Na_2CO_3 re-precipitation (Han et al., 2020). Li precipitation is modeled via a molar precipitation yield (SF_{Li_rec}), which indicates the moles of Li precipitated with respect to its moles in input. It is also assumed that the pH of the solution coming from the co-precipitation step is so high that almost all CO_3^{2-} ions added do not turn into HCO_3^- ions, permitting Li_2CO_3 precipitation.

Sintering is the final step in which precursors are thermally treated to achieve the final product. The main reaction is the calcination and lithiation of transition metal hydroxide into the selected cathode chemistry, e.g., NMC-111, whereas it is assumed that no secondary reactions occur.

3. Simulation case studies

3.1. Performance indicator definition

As anticipated in the previous section, the potential of the proposed modeling framework can be multiple. The aim in this work is to perform a quantitative analysis of the two recycling processes modeled to, eventually, evidence criticalities and open research questions that should be addressed. To perform such an analysis, common metrics need to be defined. Specifically, recycling performance indicators that, as the name suggests, allow for an evaluation of the quality of the recycling processes on a mass basis, as adopted here. In this study, the selected indicators are the Material Yield (MY) and the Battery Recovery Yield (BRY), defined as in Eqs. (2) and (3) (adapted from Vassart, 2013).

$$MY_i = \frac{M_{i,out,\ rec}}{M_{i,in}} \tag{2}$$

$$BRY = \frac{\sum_i M_{i,out,rec}}{M_{in}} \tag{3}$$

Both MY and BRY are metrics used to assess the amount of recovered materials from LIBs compared to the input mass of these batteries (M_{in}). However, they differ in their calculation methods. MY is based on evaluating the fraction of a single material "i" recovered in all the output streams considered accountable for recycling ($M_{i,out,\ rec}$). Thus, MY_i represents the mass of the specific material "i" recovered over the mass of such a material entering with the LIB input feed, $M_{i,in}$. On the other hand, BRY refers to the total mass of all recovered materials combined and expressed as a percentage of the mass of the spent LIBs entering the process. This metric provides a holistic view of the overall recycling efficiency. It is to be stressed that the mass of the output fractions considered for these indexes is expressed on a dry basis, that is, without accounting for any moisture content; oxygen is considered transparent both in input and outputs, i.e. it enters neither in M_{in} nor in $M_{i,out,\ rec}$ because such a chemical element is arguably irrelevant for the battery value chain. Clearly, such definitions come also with different questions and multiple calculation options, such as: on which basis a stream is classified as "accountable for recycling", which constitutes the list of input materials determining the reference basis for BRY calculation, and what are the restrictions on the quality of outputs, if any.

To perform a fair analysis of the processes, a few assumptions should be considered when reading the results in the next sections. Criteria for determining whether a material stream is attributed to recycling or not rest upon specific principles. Firstly, streams comprising gases/vapors or wastewater are excluded from recycling considerations as their treatment lies outside the scope of the LIBs supply chain. Secondly, streams characterized by a significant dispersion of materials, i.e., with a predominant mass fraction below 50 %, are assumed to require further processing through various unit operations; consequently, these streams are not directly designated for recycling. Hence, the slag and flue gas streams exiting from the smelter in the pyrometallurgy-based route, as well as the light plastics fractions within the hydrometallurgy-based pathway, are currently categorized as non-recyclable due to these criteria. Nevertheless, research and technological advancements in recovering materials from these streams can render them accountable for recycling in future studies. A complete overview of the streams assumed to be accountable for recycling in this study is reported in Table 2. It should be stressed that, following the original aims of the LithoRec process, output streams as recovered electrolyte and graphite are considered accountable for recycling in this case study to highlight the recycling potential of a (future) hydrometallurgical process, despite these streams rarely re-enter the battery value chain according to the current industrial practice.

When a stream is labelled as recycled without further specifications, all the materials included in it are considered accountable for calculating the performance indexes. This means, for example, considering accountable for recycling also small quantities of Co or Ni in various streams where they represent impurities. However, we can discriminate a recovered material defining it as accountable for recycling only if its mass fraction is above a certain threshold, referred to as the Purity Level (PL). When considering PLs, the values of $M_{i,out,\ rec}$ for the calculation of MY_i in Eq. (2) and BRY in Eq. (3) include only the streams where the specific material satisfies the PL threshold. Notable exceptions to this PL constraint are the streams obtained from disassembly (for the pyrometallurgy-based route in Fig. 2a) and mechanical separations (for the hydrometallurgy-based route in Fig. 2b). As a matter of fact, the recovery of the streams exiting the mechanical separations is technically well developed; thus, even components with low mass fractions can be further separated and collected, potentially allowing the recovery of all the individual materials treated (Kim et al., 2021).

Table 2
List of the output streams for both routes, pyrometallurgy-based on the left and hydrometallurgy-based on the right. Each stream is labeled as accountable for recycling (✓) or not (✗) according to the considerations expressed in Section 3.1. See Fig. 2 for the notation of the name of the streams.

Output streams (*Pyrometallurgy-based*)	Accountable for recycling	Output streams (*Hydrometallurgy-based*)	Accountable for recycling
Disassembled more valuable fraction	✓	Lower value disassembled fraction	✓
Disassembled less valuable fraction	✓	Higher value disassembled fraction	✓
Smelter flue gas	✗	Inert crushing off gas	✗
Slag	✗	CO_2 purge from electrolyte extraction	✗
Unleached metals	✗	Recovered electrolyte	✓
SO_2 flue gas	✗	Steel fraction	✓
CuS	✓	Aluminum casings fraction	✓
$Fe(OH)_3$	✓	Light plastics fraction	✗
$Ni(OH)_2$	✓	Copper foils fraction	✓
Evaporated H_2O from concentrator	✗	Aluminum foils fraction	✓
Evaporated H_2O from crystallizator	✗	Graphite and unleached	✓
Hydrated $CoCl_2$	✓	Impurities	✗
Neutralized wastewater	✗	Off gas from coprecipitation	✗
		H_2O evaporated for NMC hydroxide drying	✗
		Recovered Li_2CO_3	✓
		H_2O evaporated for Li_2CO_3 drying	✗
		Off gas from first sintering step	✗
		Off gas from second sintering step	✗
		Re-sintered NMC	✓
		Neutralized wastewater	✗

With these considerations, the next sections provide an analysis of the two recycling processes, varying the input of spent LIBs processes, and identifying the unit operations that mostly affect the aforementioned performance indicators. For the sake of brevity, the following shortcut notation is applied for the rest of the work: “Pyro” for the pyrometallurgical Umicore process in Section 2.2, “Hydro” for the hydrometallurgical co-precipitation LithoRec process in Section 2.3.

3.2. Robustness analysis

3.2.1. Pyro vs Hydro with the same feed

In this section, a quantitative analysis of the selected reference Pyro and Hydro processes presented in Section 2 is performed, considering the proposed recycling performance indicators MY and BRY introduced in Section 3.1. Table 3 summarizes the MYs and BRY values for the most relevant materials inside a LIB, providing insights into the recycling performance of the processes. Values in Table 3 are obtained by running the simulation model with a feed of spent LIBs denoted as EuroMix, whose composition is given in the caption of Table 3. This composition reflects the predicted spent LIBs flow expected in 2025 in EU (Huisman and Bobba, 2021).

Table 3 highlights that the Pyro process achieves significantly lower recycling indicators than the Hydro process. It is important to stress that these numerical results are intricately tied to the assumptions stated in Sec 3.1 and the formulation of performance indicators as in Eqs. (2) and (3) (European Commission, 2023). Therefore, these numbers should be interpreted as values derived from specific considerations that may be subject to revision. More specifically, the analysis of Table 3 enables a close insight into the capabilities of the two main recycling routes.

Focusing on the MY of specific materials, Fe is recovered almost completely by both recycling processes. Other relevant metals, such as Cu, Co, and Ni, are recovered with efficiencies which would meet the 2025 EU targets and, in some cases, the more ambitious 2030 targets (European Commission, 2023; Huisman and Bobba, 2021). Al and Mn are recovered with extremely high efficiency by the Hydro process, while their MY values are sensibly smaller for the Pyro ones since Al and Mn end up in the slag, which is considered here as a material output not accountable for the recycling efficiency due to its potential use only in the construction industry market (therefore out of the closed loop of battery grade products). The same consideration applies to Li, whose MY is ca. 80 % in the Hydro process, compared to the 0 % MY of the Pyro one where Li is contained in the slag and smelter flue gas, which are not considered recycled streams. The difference between the two processes can also be appreciated by comparing the mass of Li recovered in

Table 3
MY and BRY of representative Pyro (orange) and Hydro (blue) processes obtained via modeling simulation for the 2025 EU flow of spent batteries (EuroMix). The EuroMix flow consists of 75 % of large battery formats (out of which 88 % NMC, 1 % LFP and 11 % NCA) and 25 % of small battery formats (out of which 56 % NMC, 1 % LFP, 1 % LMO and 42 % LCO). The full battery composition is reported in Table S3 in the SI. While calculating the BRY values, the oxygen content in the spent LIBs is considered transparent.

Material	MY [wt.%]	
	Pyro	*Hydro*
Fe	83.4	98.1
Plastics	25.3	74.3
Al	55.9	99.3
Cu	91.8	95.9
C*	0.0	100.0
Li	0.0	80.3†
Co	84.8	100.0†
Mn	0.0	100.0†
Ni	96.6	100.0†
Electrolyte solvents	0.0	90.7
BRY [wt.%]	49.9	96.0
$\frac{\text{kg high quality Li recovered}}{\text{ton of spent LIBs}}$	0.0	7.5
$\frac{\text{kg high quality Co recovered}}{\text{ton of spent LIBs}}$	28.7	27.7
$\frac{\text{kg high quality Ni recovered}}{\text{ton of spent LIBs}}$	42.5	36.0

* C is considered totally separated in the Hydro process but only 85.3 % ends up in "Graphite and unleached" stream which is considered recyclable.
† Li, Co, Mn, and Ni are present in the sintered cathode material but also in other streams as impurities. As a matter of fact, only 58.7 % of Li and 81.8 % of Co-Mn-Ni end up in the new NMC111 cathode.

high-quality output streams per ton of spent LIBs, where high-quality here refers to the potential to be reused as a battery-grade precursor for the manufacturing of new batteries (Latini et al., 2022): by following the Pyro process, no high-quality Li is recovered, while the Hydro process has the potential, at industrial scale, to generate ca. 7 kg of high-quality Li per ton of spent LIB, which can be reintroduced in the battery production chain. On the other hand, the mass of high-quality Co and Ni per ton of processed spent batteries is equal, or even slightly lower, for the Hydro process, if compared to the Pyro one for the same LIB feed. This is attributed to the losses introduced by mechanical separations required by the hydrometallurgy-based route, especially the sieving and the detachment of active materials from current collector foils, which are identified as major bottlenecks of this process (Ciez and Whitacre, 2019). It is also worth noting that in the Hydro process the mass of high-quality Co and Ni is in contrast with the MYs of such metals, which are equal to 100 % for both metals. This implies that a certain fraction of Co and Ni in the Hydro process is only present as impurities in other streams. Conversely, even if the MYs of Co and Ni in the Pyro process are 84.8 % and 96.6 %, the bottom part of Table 3 indicates that such metals are recovered here with higher quality.

On the other hand, the MY indicator can highlight the difference between Pyro and Hydro processes when plastics, electrolyte and graphite recovery rates are analyzed: considering that these materials are mostly burnt in the Pyro process, the values in Table 3 highlight the potential of the hydrometallurgical route to enable significantly larger MYs for these materials.

Considering the MYs reported in Table 3, the BRY of the reference Pyro process is ca. 50 %, while the hydrometallurgical route can potentially lead to larger BRY values, even above 90 %, due to the ability of the selected Hydro process to recover graphite and part of the electrolyte. It is emphasized that the examined Hydro process represents a desirable future direction for the hydrometallurgical-based route, rather than the current industrial situation in which recovered graphite and electrolyte are still used for energy recovery along with other plastic materials. Nevertheless, it must be stressed out that all the numbers in Table 3 are strictly linked to the assumptions stated in Section 3.1; if one would consider the slag as accountable for recycling, the BRY for the Pyro route would jump to around 70 %. Indeed, all the Al not recovered in the disassembly phase (foils and fractions) remain stuck into the slag representing the major component there contained.

To further delve into the discussion made for Table 3, it is interesting to analyze how recycling performance indicators change when relaxing the assumption that everything contained in a stream accountable for recycling is considered recovered, regardless of its mass fraction in the stream. This is possible by introducing the PLs into the calculation of recycling indicators. PLs are defined as the lower limits of the mass fractions of the materials so that they can be considered recycled; in other words, a material is labeled as an impurity (and thus not accountable for recycling indicators) if its mass fraction in the stream is less than the purity level.

By adopting the PL criterion, the values of recycling performance indicators can only be smaller or equal than those reported above. Clearly, the higher the PLs required, the lower the values of the recycling indicators. As already specified in Section 3.1, PLs are only applied to output streams starting from smelting (for Pyro) or leaching (for Hydro), while they are not applied to streams exiting from disassembly and mechanical operations. Results of such an analysis are shown in Fig. 3. The scattered columns represent the same values reported in Table 3 and show a clear distinction from the plain colored columns which consider PLs = 0.9.

Fig. 3 shows that, with the introduction of PLs, the Pyro route exhibits a slightly lower BRY, which is attributed to the minor decrease in the recovery of Cu, Co, and Ni. Specifically, it is crucial to note in the Pyro process that the recovered copper (mainly as CuS), cobalt (mainly as $CoCl_2$), and nickel (mainly as $Ni(OH)_2$) are recycled with a high degree of purity, respectively of 100.0 %, 92.4 %, and 98.5 %. The precipitation of $NiCl_2$ is responsible for the impurities in the $CoCl_2$ stream, whereas impurities in the $Ni(OH)_2$ stream results from the precipitation of other metal oxides. For this reason, the use of PLs does not lead to drastic reductions in the original results for the Pyro process.

Upon introduction of PLs, the Hydro route maintains higher recycling indicators compared to the Pyro process, despite exhibiting a more pronounced decrease in both MYs and BRY. In the hydrometallurgy-based route, Cu is mainly recovered in the mechanical section, notably in "Cu foils fractions" stream (~86 %), but it is also present as an impurity in "Al casing fractions" (~6 %) and in "Al foils fractions" (~4 %) (see Fig. 2b for reference to the stream names). Since we assume that PLs do not apply to the material recovery of streams exiting from mechanical separations, the Cu MY in Fig. 3 remains unchanged upon the introduction of PLs; on the other hand, should PLs be applied to all the streams, the Cu MY would decrease from 96 % to 86 %. Instead, Li, Co, and Ni are primarily recovered in the cathode material for high-cobalt cathodes (~59 %, ~82 %, 82 %), but they also exist as impurities in "Al foils fractions" (~15 %). Li is directly recycled to the sintering step as Li_2CO_3 to produce NMC-111; however, it should be noted that NMC-811 production would require $LiOH{\bullet}H_2O$ as a Li source in the sintering step (Kim et al., 2017). This implies that, in this case, either (i) recovered Li exits the process as precipitated Li_2CO_3 in the Li recovery step while $LiOH{\bullet}H_2O$ is added in the sintering step to obtain NMC-811; or (ii) the Li recovery step must be modified in the process to produce lithium hydroxide. Fig. 3 also reveals that BRY varies significantly after using PLs, explained by the fact that the "Graphite and unleached" stream is no longer considered recycled since all the mass fractions of the materials are lower than the fixed PLs.

Lastly, it is evident that even though the hydrometallurgy-based route can achieve high MY and BRY values, these are significantly impacted when PLs are considered. This indicates that, in the Hydro process, materials are more distributed along the output streams, while in the Pyro process, despite smaller MYs and BRY, the quality of the recovered materials is high, reflecting a minor sensitivity to the PLs. It should be emphasized again that these figures result from modeling

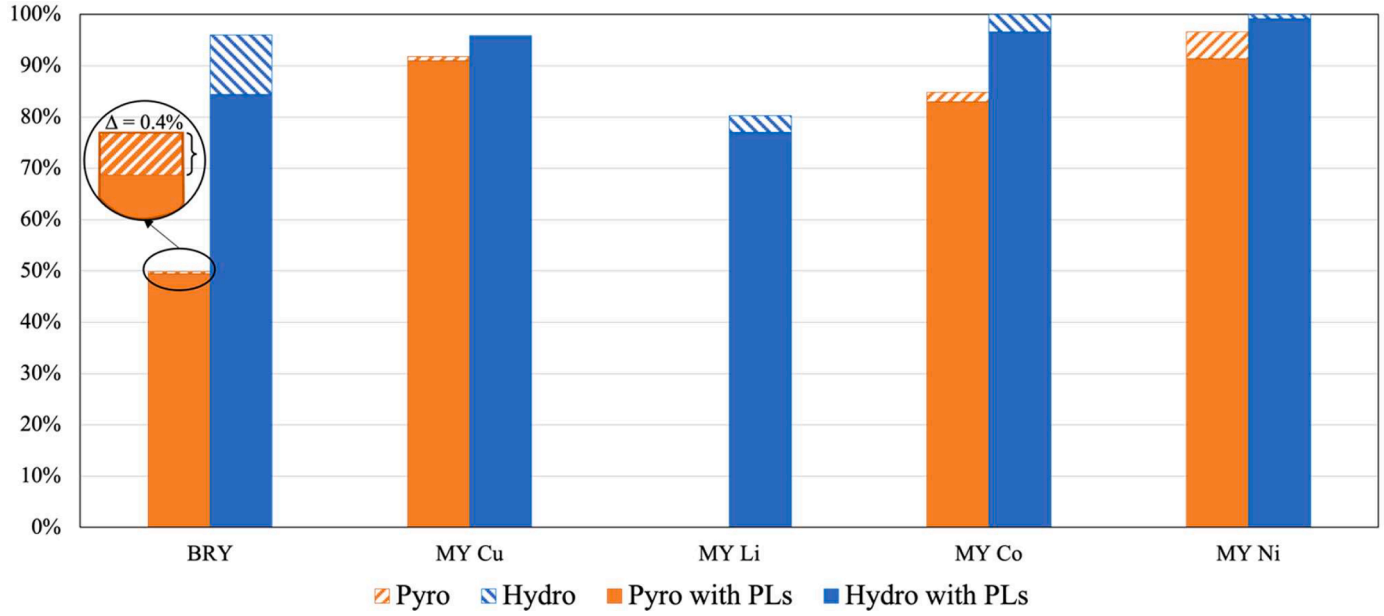

Fig. 3. Values of material (MY) and recycling (BRY) yields of the two routes reported also in Table 3, highlighting the effects of the use of the PLs = 0.9 in the calculation of the performance indicators. The inset shows for the Pyro route the difference (Δ) between the two BRY values.

simulations with a specific choice of what is considered accountable for recycling or not (see Table 2) and the selection of an arbitrary threshold for the PLs. Furthermore, we are referring to a (future) hydrometallurgical process which has the potential, at industrial scale, to provide recycled streams at sufficient quality to the re-enter the LIB value chain, thus going beyond the current industrial practice.

3.2.2. *Effect of different LIBs chemistries*

The panorama of spent LIBs requiring treatment in the coming decades is vast and variable. This necessitates an analysis on the robustness of the two modeled recycling routes to accommodate different spent LIBs chemistries entering the process. The robustness is still assessed using the chosen recycling indexes, namely, MY and BRY, without considering purity levels.

Fig. 4 shows the deviations from the indexes reported in Table 3, obtained by feeding the two processes with different types of single-chemistry batteries: NMC-111, NMC-622, NMC-811, and LFP (only for Pyro). As already anticipated in Section 2.3, when the Hydro process is fed with a specific NMC chemistry, the re-sintered cathode considered is always the corresponding NMC in input, except for LFP, which cannot be produced via co-precipitation. Deviations of Co MYs are not reported, as these values are negligible for all types of feed in both processes. However, in the Pyro route, Co is recovered in a stream with $NiCl_2$ as its main impurity. Therefore, even if the Co MY is independent for different inputs, the purity of the product $CoCl_2$ decreases as the percentage of Ni in the cathodes of the spent LIBs entering the process increases, i.e. passing from NMC-111 to NMC-811. Similarly, no deviations are reported in the Hydro process for Cu and Ni, whose purity remains unchanged.

It should be noted that an input feed consisting only of LFP batteries is not considered for the simulated hydrometallurgical process (LithoRec). As described in Section 2.3, leaching of LFP leads to the undesired precipitation of insoluble metal phosphates, resulting in the loss of valuable metals during the co-precipitation step of some Hydro processes. Furthermore, when feeding only LFP, there is no Co, Ni, and Mn for the co-precipitation of the ternary NMC precursor. This indicates that LFP shall not be the primary goal for the Hydro process, except in small quantities when NMC or other chemistries are present (as in the EuroMix). Moreover, as detailed in several studies (Latini et al., 2022; Wasesa et al., 2022), battery recyclers may not accept LFP batteries due to lower

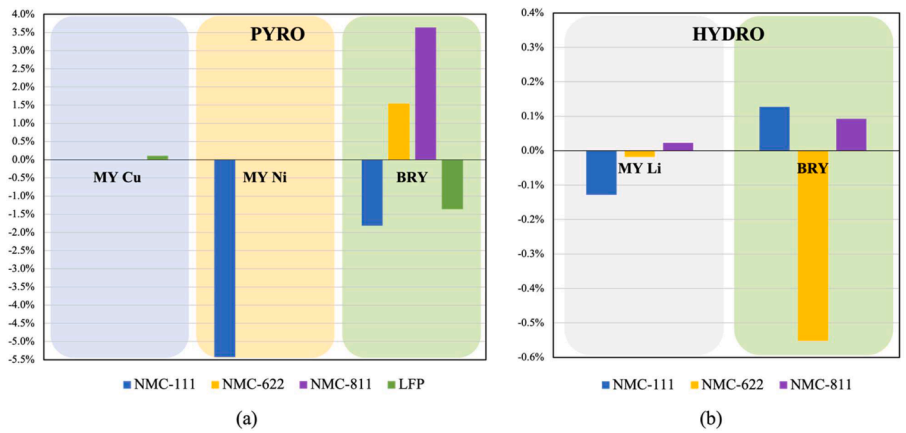

Fig. 4. Deviations from the results obtained using EuroMix as input in Pyro (a) and Hydro (b) routes. Different colors represent the deviations achieved feeding different inputs to the two recycling routes: NMC-111 (blue), NMC-622 (yellow), NMC-811 (purple) and LFP (green, only for Pyro, see Section 2.3). Note also that the scales of the figures are not the same, evidencing the different impacts of LIBs chemistries on the two routes.

economic revenues compared to Co- and Ni-containing chemistries. Therefore, the presence of LFP batteries in the feed of hydrometallurgical and co-precipitation processes should be restricted as much as possible, not only for economic reasons but also for technological limitations.

Comparing the indicators of the Pyro route obtained for different inputs (Fig. 4a), changing the LIB chemistry share in the input feed affects MYs and BRY. Fig. 4a shows that when considering the NMC-111 case, the deviation of Ni MY is negative (−5.5 %), highlighting that process conditions should be modified when feeding only NMC-111 spent batteries compared to the EuroMix input to favor Ni precipitation. Failure to do so may result in Ni losses up to 5.5 % and a 2 % decrease in BRY. On the contrary, there is no deviation for Ni MY with NMC-622 and NMC-811 as inputs, and the purity of the salt remains constantly high (99.5 %) as the amount of Ni precipitated as $Ni(OH)_2$ returns to the original case or even increases given the abundance of Ni ions. Accordingly, BRY values when considering NMC-622 and/or NMC-811 are higher despite Ni MY and Co MY do not change. This increase in BRY is explained based on MYs values: since Ni MY is greater than Co MY, the use of low Co cathodes as inputs results into greater total mass recovery, hence a greater BRY. Instead, BRY for LFP input is slightly lower because more mass of Fe ends up in the slag generated in the smelter, thus decreasing the total mass recovered.

Fig. 4b depicts even more negligible numerical deviations for the Hydro process with respect to those obtained in the Pyro route; as a matter of fact, no deviations are reported for Cu and Ni. However, due to the use of different chemistries of the produced cathode, slightly different Li recoveries are shown. Yet, this is not the reason of the marginal increase in BRY for NMC-111 and NMC-811 input feeds, which is due to a slightly greater recovery of Fe and Al in the mechanical and impurities removal section, which does not happen with NMC-622 as input. This is simply due to minor differences in the LIBs mass compositions.

In summary, the Pyro route exhibits higher sensitivity to varying input feeds concerning BRY. It is essential to note that no alterations are made to the operating conditions set for the EuroMix input when experimenting with different chemistries of spent LIBs. However, there is still potential for further enhancing BRY and MYs values by optimizing process parameters or adjusting reactant stoichiometries accordingly. Nonetheless, the recent proposition for battery recycling regulation by the European Commission mandates that all collected waste batteries undergo appropriate treatment and recycling (European Commission, 2023). Therefore, it becomes imperative to develop effective strategies to enable the effective recycling of different battery chemistries, particularly those with lower economic value.

3.2.3. *Effect of different share of large format LIBs*

A factor that strongly impacts the BRY of the pyrometallurgy-based process is the share of large battery systems vs. small format LIBs in the feed. As a matter of fact, housings, electronics, cables, and other peripherical components account for up to 45 % of the weight of a large battery system (refer to Table S3 in the SI for the compositions used in the simulations). These parts can be easily dismantled and recovered in the pre-treatments section, resulting in a rise of the BRY. Conversely, for small-format LIBs, the outer casing is not considered part of the battery itself and is excluded from the BRY calculation. To quantitively analyze these considerations, the influence of the mass percentage of large batteries within the input on the BRY is shown in Fig. 5, using the EuroMix chemistry compositions as a reference input feed to the processes.

Fig. 5 confirms that the pyrometallurgical route is more responsive to variations in the percentage of large batteries in input. With a lower BRY than the Hydro route, the recovery of the pack and cell housing materials significantly contributes to the index calculation. To give an idea, for the reference case, (EuroMix at 75 % large batteries as input, indicated by the green dash-dotted line in Fig. 5), the material “Electronics & Cables” is responsible for 8 % of the BRY obtained in the Pyro route and for 4 % of BRY obtained in the Hydro one. Thus, if a general pyrometallurgical process treated only small-format LIBs, it would barely achieve a BRY of 40 %, according to the given definition, evidencing how excluding the outer casing of small-format LIBs in BRY eventually leads to its lowest value.

In summary, this analysis highlights that BRY and MYs are valuable metrics to assess the general capability of a recycling process and its sensitivity to different input battery feeds, enabling a distinction between different recycling routes. In addition, the analysis also reveals that special care should be taken in harmonizing the BRY calculation regarding the outer casing and in comparing the quality of the recovered streams considering the targets on recycling contents.

3.3. *Sensitivity analysis*

To conclude the examination of the two modeled recycling processes, a pertinent inquiry pertains to the identification of pivotal unit operations that exert significant influence over the MYs and BRY values. Within this analytical framework, the employment of a sensitivity analysis emerges as an effective tool to elucidate the most sensitive operating parameters of the recycling routes, delineate critical unit operations, and discern the process conditions that yield the greatest impact on material recovery outcomes.

The setup chosen in this study is the following. Each parameter in the process simulation code has been individually varied by ±10 %. Clearly, this range is restricted for those cases where such a variation would set a

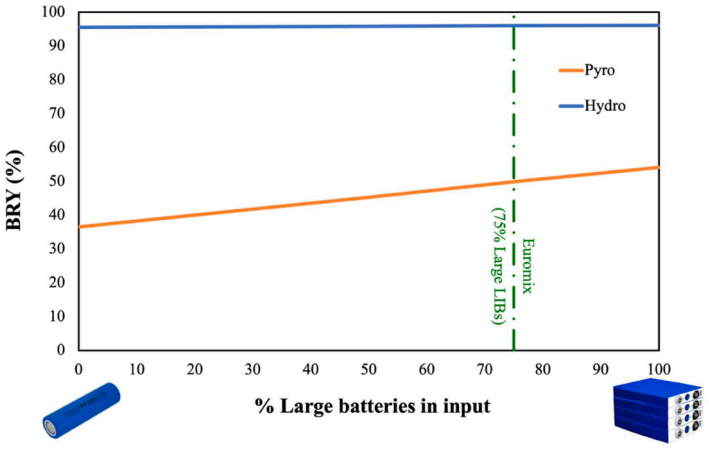

Fig. 5. BRY as a function of the mass fraction of the large batteries present in the input feed to the two processes. The green dash-dotted line represents the reference input as treated in Table 3.

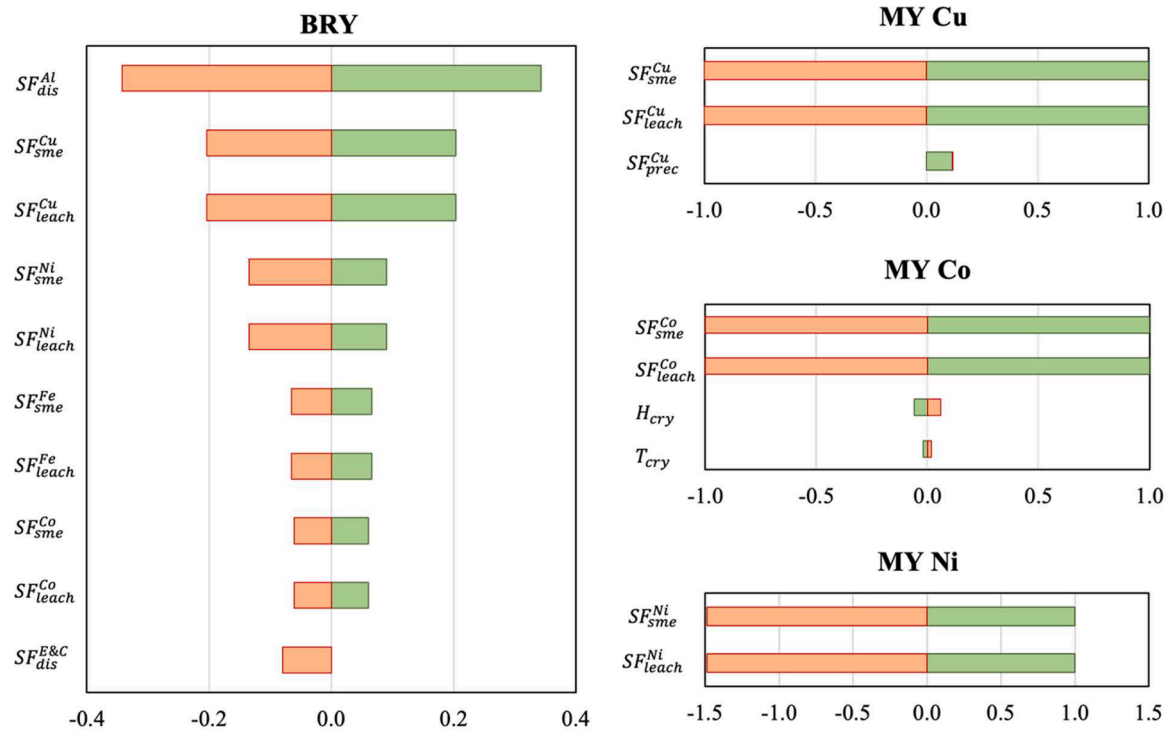

(a)

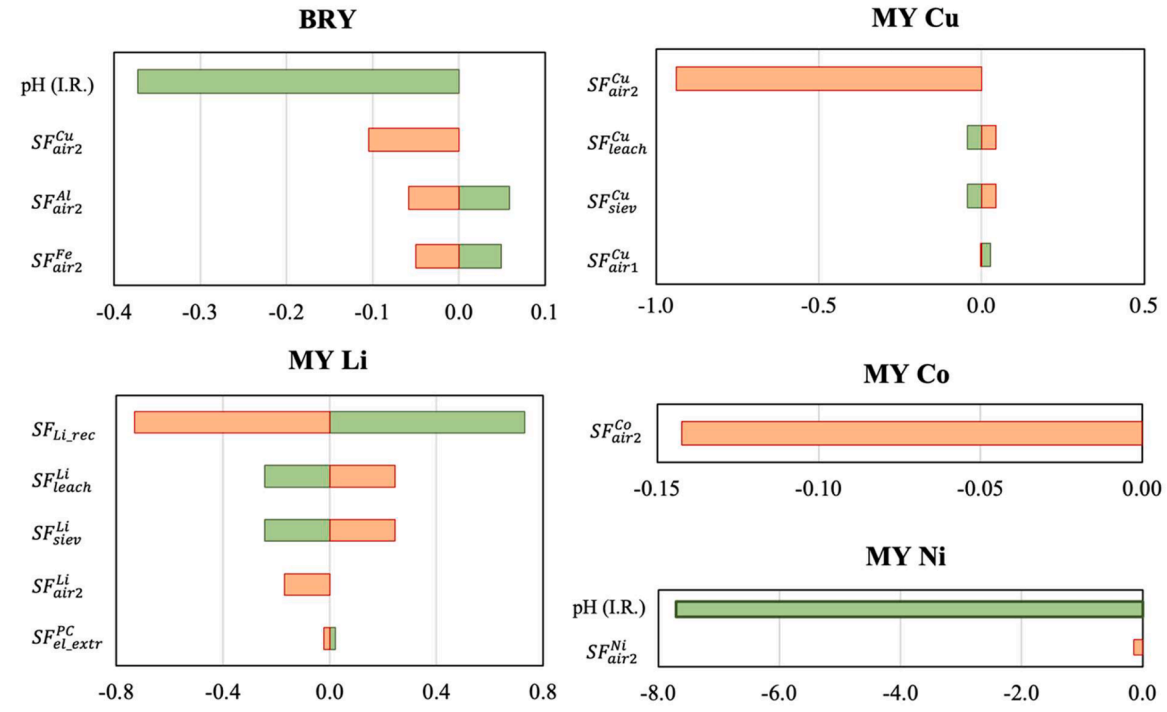

(b)

Fig. 6. Sensitivity analysis of BRY and MY of some of the CRMs for the (a) Pyro and (b) Hydro processes with EuroMix feed. In the tornado plots, the sensitivity factors are reported in green bars for a positive variation of the parameter analyzed and in red for a negative variation. The reader can refer to Section 2 for the list and meaning of symbols.

parameter beyond its physical and/or technical boundaries. In practice, each parameter has been changed one at a time, so all the simulations performed have the same parameter values except for the one modified, maintaining fixed input feed conditions (i.e. EuroMix). After recording the variation in MYs and BRYs in response to alterations in the selected parameter, these changes have been normalized to ascertain their sensitivity factor; upon such normalization, a sensitivity factor of 1 indicates a direct sensitivity. It should also be noted that, in general, a positive variation of a process parameter does not necessarily lead to a positive variation of the recycling performance indicator, i.e., negative

sensitivities are possible. In any case, the magnitude of the normalized sensitivity factor highlights whether a specific parameter is critical or not.

Fig. 6 shows the most representative sensitivity factors for the two processes analyzed. Almost all the parameters that influence the recycling yields the most are the SFs of a few unit operations. In Fig. 6a, for the Pyro route, a direct correlation exists between SFs in the smelter and in the leaching of the alloy for the Ni and Co MYs (i.e., sensitivity factor equal to 1). This means that these parameters are extremely important for the recovery of those materials because they directly affect the composition of the streams that undergo further chemical treatments. In the hydrometallurgical route (Fig. 6b), the pH value in the impurities removal step, pH (I.R.), greatly affects the Ni MY, since $Ni(OH)_2$ solubility decreases with the increase of pH. In this case, the sensitivity factor is very high, equal to ca. 8 in absolute value. It is interesting to underline that the second air classification step (η_{air2}) is another unit operation always present with non-negligible sensitivity factors. As a matter of fact, the output stream for this operation is "Light plastics fractions", which contains different CRMs as impurities and is not considered accountable for recycling. This means that when varying the SF_{air2}, MY of Ni, Co, and Li are directly impacted, deviating such components in streams where they are recovered or not. Clearly, the magnitude of such deviation strictly depends on the value of the corresponding SF.

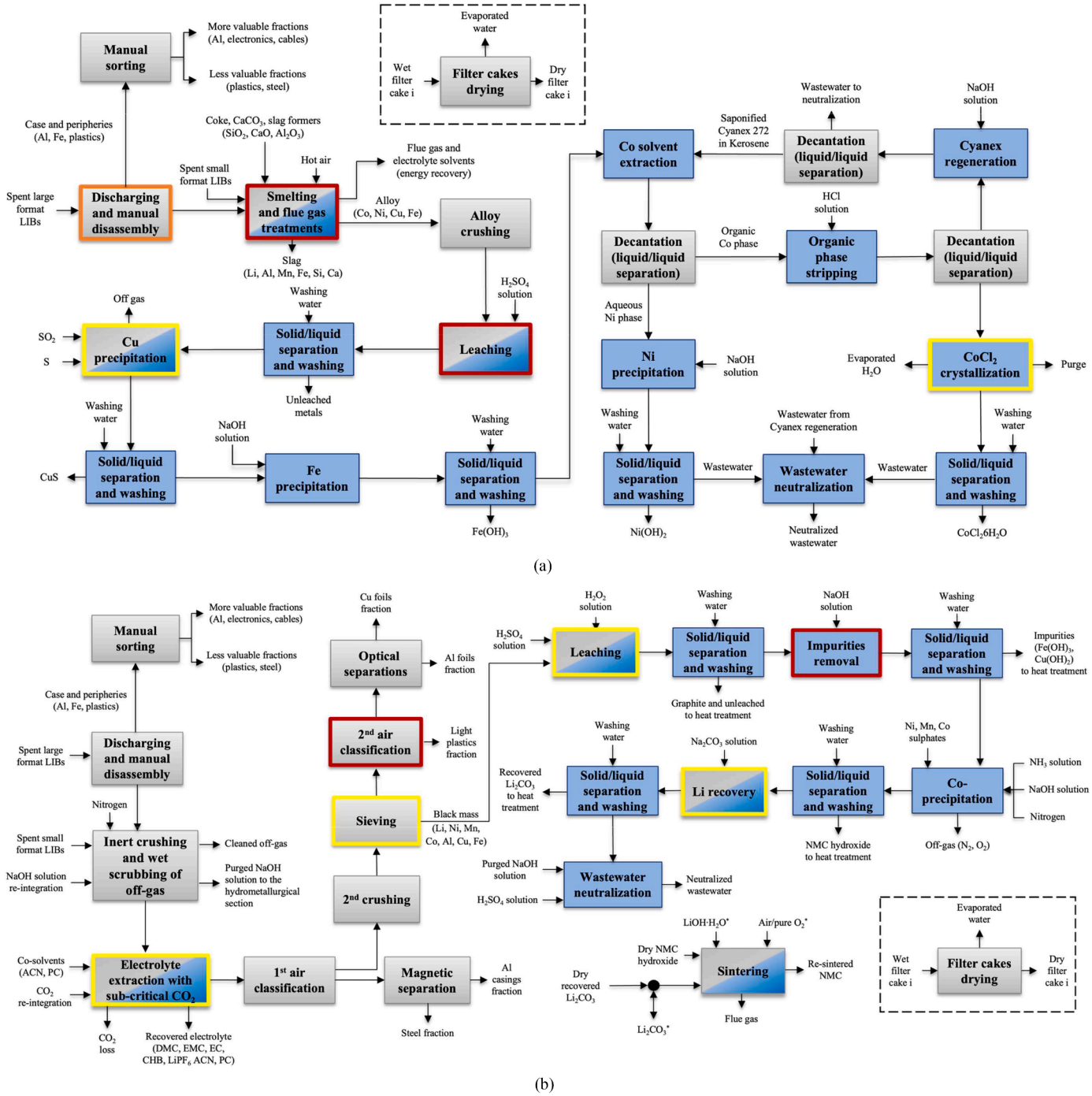

Fig. 7. Block diagrams of the (a) Pyro and (b) Hydro processes evidencing the unit operations whose parameters impact recycling yields the most, divided into three sensitivity levels: yellow for unit operations where a parameter shows a sensitivity factor for MYs of CRMs greater than 0.01 in absolute value; orange for unit operations where a parameter shows a sensitivity factor for BRY greater than 0.05 in absolute value; red when both conditions above are fulfilled.

By exploiting results from the sensitivity analysis, it is now possible to identify which operations are the ones most affecting the recycling indexes. An analysis between the two modeled routes can be made based on three *sensitivity* levels depending on how severe the MYs of CRMs or BRY are affected by the parameter change as in Fig. 7.

Both routes have two unit operations marked with red, influencing both MYs of CRMs and BRY. For Pyro these units are "Smelting" and "Leaching"; this is clear given their black-box core that establishes a linear relation between the SF value and the corresponding MY calculated on the outputs of those operations. On the other hand, for the Hydro route, both "2nd air classification" and "Impurities removal" are marked in red. As discussed for Fig. 6b, varying SF_{air2} has a significant impact on both the considered metrics, as also reported in the literature (Ciez and Whitacre, 2019; Latini et al., 2022). On the other hand, the sensitivity factor of the pH(I.R.) is responsible of all the Fe and Cu precipitated as hydroxides, therefore removing impurities. The "Discharging and manual disassembly" step proves crucial only for the calculation of BRY in the Pyro process, as it is marked with orange in Fig. 7a. This remarks what already discussed about Fig. 5: being the mass of pack and cell housing recovered in this operation quite relevant, the SFs used for disassembly (SF_{dis}) have a direct impact on the mass recovered but, at the same time, do not affect any CRM contained in the battery cells. A main difference that can be also underlined is that Fig. 7a shows only two blocks marked with yellow ("Cu precipitation" and "$CoCl_2$ crystallization"), whereas in Fig. 7b, there are four unit operations marked as yellow blocks ("Electrolyte extraction", "Sieving", "Leaching" and "Li recovery"). This can be explained by the fact that the Hydro route recovers more metals than the Pyro one, including Li. Therefore, it is possible to state that the recycling performance of the Hydro route is sensitive to a greater number of parameters than the Pyro one. This assertion is substantiated by the nature of hydrometallurgical processes, which, involving multiple sequential unit operations, such as leaching, impurity removal, and precipitation, collectively represent a complex network. Each of these operations is inherently influenced by specific chemical, physical, and thermodynamic factors. For instance, variations in parameters like pH, temperature, and reactant concentrations can significantly impact the efficiency of leaching or precipitation reactions. Furthermore, the heterogeneous composition of spent LIBs and the Hydro route's reliance on precipitation steps to separate different materials introduce additional variables. The mechanical separation section in the Hydro process adds another layer of complexity, involving numerous steps such as disassembly, classification, and impurities removal. Each of these steps represents a potential point of influence and variation in the recycling process, demanding careful control to avoid faults or deviations from optimal performance and to guarantee high recycling indicators. In contrast, the Pyro processes, while not devoid of complexities, typically involve fewer sequential steps. The sensitivity to operational parameters in pyrometallurgy may be comparatively less intricate, considering its thermal processing nature, like smelting. However, it is essential to note that the use of a "black box" approach in Pyro units indicates a certain level of intricacy, and assumptions might not be straightforward due to the nuanced aspects of the process, even if concentrated within a single unit. In any case, this increased sensitivity in the Hydro not only underscores the complexity of its processes but also points to the rich opportunities for research and optimization. It beckons the exploration of how different parameters interplay within the intricate network of unit operations and how fine-tuning them can enhance the overall recycling performance.

Lastly, one crucial aspect requires attention in relation to this sensitivity analysis. Several factors play a role in shaping the outcomes just examined, including the criteria used to determine *sensitivity* levels, and the calculation method for the chosen performance indexes. However, the most pivotal factor is the determination of which material streams are deemed responsible for recycling (i.e., Table 2). All the insights drawn from this analysis are intricately tied to the specific selection of recovered streams and their compositions. Modifying this selection would necessitate a fundamental shift in the underlying framework of the sensitivity analysis, prompting the need for a fresh analysis to accurately reflect the new configuration. Therefore, as already stressed in this study, the proposed modeling framework itself can deliver quantitative results, albeit such numerical values are not absolute but just derived from the considerations stated and that can be open to changes. From a policy and industrial decision-maker perspective such statements clearly point in the direction of developing harmonized rules and definitions to assess what can be considered recycled. As a matter of fact, and in line with the recent European regulation (European Commission, 2023), neither a qualitative nor a quantitative analysis of the LIBs recycling routes can deny the importance of establishing indicators and calculation rules to quantify yields that can ensure both quantity and quality of recycled outputs to enhance a closed loop of battery-grade materials.

4. Conclusions

The study delved into the modeling of lithium-ion battery (LIB) recycling, focusing on a pyrometallurgy-based route and a hydrometallurgical one with co-precipitation of the precursor of cathode active materials, using a Python-based quantitative process simulator. Rather than directly comparing these inherently distinct processes, the primary aim was to provide an analysis of their performance robustness. As highlighted in the key findings, the study aimed to offer quantitative insights and complement the discussion presented in a recent review paper (Latini et al., 2022). Firstly, the study emphasized the pivotal role of defining what is considered accountable for recycling and what is not, recognizing that the numerical outcomes of recycling performance indicators are closely tied to these definitional choices.

Secondly, the introduction of Purity Levels (PLs), representing mass fraction thresholds for material to not be classified as impurities in a stream, was identified as a critical factor. The study discerned that the impact of PLs was more pronounced on the hydrometallurgical route than on the pyrometallurgical one, underscoring the importance of considering these thresholds in the evaluation of recycling performance.

Thirdly, the share of large vs. small format LIBs has a more significant effect on pyrometallurgical route performance than on the hydrometallurgical process. In addition, varying the chemistry of the spent LIBs entering the recycling routes does not considerably affect the recycling indexes of both processes; however, it must be stressed that optimizing the operational parameters according to the composition of the spent battery feed is still fundamental to reduce the utilities consumptions and increase the process performance.

A dedicated sensitivity analysis identified the sections of the recycling processes which affect the recycling yields the most. The hydrometallurgy-based route is characterized by a larger number of sensitive unit operations compared to the pyrometallurgy-based one. This result implies that the hydrometallurgy-based route has a larger number of unit operations intertwined and influenced by various factors demanding meticulous control over specific operational parameters. Simultaneously, it paves the way for advanced research opportunities, prompting the exploration of the nuanced interactions and dependencies within the hydrometallurgical processes. It is important to note that these results are dependent on the choices made about what stream must be considered accountable for recycling, highlighting the need for further investigation, data acquisition, and harmonization of rules.

Despite these valuable insights, it is important to acknowledge certain limitations in the study. It must be stressed that the sensitivity of the results to the definition of what constitutes "recycled" streams underlines a level of subjectivity in the findings. Additionally, the study is confined by specific assumptions and simplifications in the modeling process, reflecting the challenges of capturing the full complexity of real-world recycling scenarios. The research is also based on publicly available information contained in scientific articles and patents, introducing

a potential for imprecisions or outdated data. Moreover, the dynamics of the LIB recycling field, subject to ongoing developments, were not comprehensively accounted for in the model, including variations in actual operational conditions, market dynamics, and evolving technologies. Hence, considering these modeling limitations, the performed sensitivity analysis serves a dual purpose: firstly, assessing the potential error bars introduced by uncertain parameters and validating them within the chosen modeling criteria; secondly, providing insights into specific unit operations to focus on for improving recycling efficiency. In particular, significant development of industrial processes is expected due to new targets regarding LIBs and lithium recovery. However, public data for these developments are not available. Therefore, the analysis presented in this work not only elucidates the current state of recycling processes but also drives research and industrial practices towards improving Li recovery. We specifically highlight the impact of Li recovery in the pyrometallurgical process, quantitatively demonstrating its influence on recycling performance indicators.

In addition, the European Union is developing metrics on recovery yields to aid the regulation of battery recycling processes (in accordance with Art. 71 of European Commission (2023)). A quantitative tool based on process simulation would in principle be required for this task and is currently missing in the literature. Therefore, we argue that our study is a first step in this direction and fills a scientific gap, fostering future improvements by the community.

In perspective, the proposed model framework holds promise for future applications, including environmental impact assessment, LCA, and potential regulatory frameworks. The model can be utilized to quantitatively assess the environmental impact of recycling routes and contribute to the development of sustainable practices in the LIB recycling industry.

5. Disclaimer

Views expressed are those of the authors and do not reflect an official position of the European Commission. Any mention of commercial companies or products in this study does not imply recommendation or endorsement by the University of Pisa, the JRC, and the European Commission.

CRediT authorship contribution statement

Marco Vaccari: Writing – review & editing, Writing – original draft, Supervision, Conceptualization. **Filippo Parlanti:** Writing – original draft, Software, Formal analysis. **Fabio M. Manni:** Validation. **Martina Orefice:** Investigation, Validation, Writing – review & editing. **Fabrice Mathieux:** Resources, Supervision. **Gabriele Pannocchia:** Conceptualization, Methodology, Writing – review & editing. **Leonardo Tognotti:** Project administration, Supervision. **Antonio Bertei:** Writing – review & editing, Conceptualization, Funding acquisition, Project administration, Supervision, Validation.

Declaration of competing interest

The authors declare that they have no known competing financial interests or personal relationships that could have appeared to influence the work reported in this paper.

Data availability

Data will be made available on request.

Acknowledgment

M.V., F.P, G.P., L.T., and A.B. acknowledge funding from the National Recovery and Resilience Plan, Mission 4 Component 2 Investment 1.3 - Call for tender No. 1561 of 11.10.2022 of Ministero dell'Università e della Ricerca, according to attachment E of Decree No. 1561/2022, Project title "Network 4 Energy Sustainable Transition - NEST", CUP I53C22001450006; funded by the European Union - NextGenerationEU. Financial support from the European Commission (Service Contract Number 724183) is also acknowledged. The authors extend gratitute to anonymous reviewers for enhancing their study.

Supplementary materials

Supplementary material associated with this article can be found, in the online version, at doi:10.1016/j.resconrec.2024.107643.

References

Arshad, F., Lin, J., Manurkar, N., Fan, E., Ahmad, A., Tariq, M.un N., Wu, F., Chen, R., Li, L., 2022. Life cycle assessment of lithium-ion batteries: a critical review. Resour. Conserv. Recycl. 180 https://doi.org/10.1016/j.resconrec.2022.106164.

Baars, J., Domenech, T., Bleischwitz, R., Melin, H.E., Heidrich, O., 2021. Circular economy strategies for electric vehicle batteries reduce reliance on raw materials. Nat. Sustain. 4, 71–79. https://doi.org/10.1038/S41893-020-00607-0.

Barai, P., Feng, Z., Kondo, H., Srinivasan, V., 2019. Multiscale computational model for particle size evolution during coprecipitation of li-ion battery cathode precursors. J. Phys. Chem. B 123, 3291–3303. https://doi.org/10.1021/acs.jpcb.8b12004.

Blömeke, S., Scheller, C., Cerdas, F., Thies, C., Hachenberger, R., Gonter, M., Herrmann, C., Spengler, T.S., 2022. Material and energy flow analysis for environmental and economic impact assessment of industrial recycling routes for lithium-ion traction batteries. J. Clean. Prod. 377, 134344 https://doi.org/10.1016/J.JCLEPRO.2022.134344.

Bobba, S., Carrara, S., Huisman, J., Mathieux, F., Pavel, C., European Commission, Directorate-General for Internal Market, I., 2020. Critical raw materials for strategic technologies and sectors in the EU : a foresight study. https://doi.org/https://data.europa.eu/doi/10.2873/58081.

Cattaneo, P., Callegari, D., Merli, D., Tealdi, C., Vadivel, D., Milanese, C., Kapelyushko, V., D'Aprile, F., Quartarone, E., 2023. Sorting, characterization, environmentally friendly recycling, and reuse of components from end-of-life 18650 li ion batteries. Adv. Sustain. Syst. 7 https://doi.org/10.1002/adsu.202300161.

Cheng, Q., Chirdon, W.M., Lin, M., Mishra, K., Zhou, X., 2019. Characterization, modeling, and optimization of a single-step process for leaching metallic ions from LiNi1/3Co1/3Mn1/3O2 cathodes for the recycling of spent lithium-ion batteries. Hydrometallurgy 185, 1–11. https://doi.org/10.1016/j.hydromet.2019.01.003.

Cheret, D., Santen, S., 2007. Battery recycling. US 7169206 B2.

Ciez, R.E., Whitacre, J.F., 2019. Examining different recycling processes for lithium-ion batteries. Nat. Sustain. 2, 148–156. https://doi.org/10.1038/s41893-019-0222-5.

Davis, K., Demopoulos, G.P., 2023. Hydrometallurgical recycling technologies for NMC Li-ion battery cathodes: current industrial practice and new R&D trends. RSC Sustain. 1, 1932–1951. https://doi.org/10.1039/D3SU00142C.

European Commission, 2023. Regulation (EU) 2023/1542 of the European parliament and of the council of 12 July 2023 concerning batteries and waste batteries, amending Directive 2008/98/EC and Regulation (EU) 2019/1020 and repealing Directive 2006/66/EC.

European Commission, 2021a. European green deal : delivering on our targets. Publications Office of the European Union. https://doi.org/10.2775/373022.

European Commission, 2021b. Horizon Europe: Strategic Plan 2021-2024.

Fan, E., Li, L., Wang, Z., Lin, J., Huang, Y., Yao, Y., Chen, R., Wu, F., 2020. Sustainable recycling technology for li-ion batteries and beyond: challenges and future prospects. Chem. Rev. https://doi.org/10.1021/acs.chemrev.9b00535.

Ferrara, C., Ruffo, R., Quartarone, E., Mustarelli, P., 2021. Circular economy and the fate of lithium batteries: second life and recycling. Adv. Energy Sustain. Res. 2 https://doi.org/10.1002/aesr.202100047.

Flett, D.S., 2005. Solvent extraction in hydrometallurgy: the role of organophosphorus extractants. J. Organomet. Chem. 690, 2426–2438. https://doi.org/10.1016/J.JORGANCHEM.2004.11.037.

Gratz, E., Sa, Q., Apelian, D., Wang, Y., 2014. A closed loop process for recycling spent lithium ion batteries. J. Power. Sources. 262, 255–262. https://doi.org/10.1016/j.jpowsour.2014.03.126.

Green, Dr.D.W., Southard, Dr.M.Z., 2019. Perry's Chemical Engineers' Handbook, Perry's Chemical Engineers' Handbook, 9th Edition. McGraw-Hill Education.

Grützke, M., Krüger, S., Kraft, V., Vortmann, B., Rothermel, S., Winter, M., Nowak, S., 2015. Investigation of the storage behavior of shredded lithium-ion batteries from electric vehicles for recycling purposes. ChemSusChem 8, 3433–3438. https://doi.org/10.1002/CSSC.201500920.

Hanisch, C., Diekmann, J., Stieger, A., Haselrieder, W., Kwade, A., 2015. Recycling of lithium-ion batteries. Handbook Clean Energy Syst. 1–24. https://doi.org/10.1002/9781118991978.HCES221.

Harper, G., Sommerville, R., Kendrick, E., Driscoll, L., Slater, P., Stolkin, R., Walton, A., Christensen, P., Heidrich, O., Lambert, S., Abbott, A., Ryder, K., Gaines, L., Anderson, P., 2019. Recycling lithium-ion batteries from electric vehicles. Nature. https://doi.org/10.1038/S41586-019-1682-5. Nature Publishing Group.

Herrmann, C., Kara, S., Kwade, A., Diekmann, J., 2018. Sustainable production. Life Cycle Eng. Manage. https://doi.org/10.1007/978-3-642-28848-7.

Hong, T., Wei, Y., Li, L., Mumford, K.A., Stevens, G.W., 2020. An investigation into the precipitation of copper sulfide from acidic sulfate solutions. Hydrometallurgy 192, 105288. https://doi.org/10.1016/j.hydromet.2020.105288.

Huisman, J., Bobba, S., 2021. "Available For Collection" study on alternative collection targets for waste portable and light means of transport batteries. https://doi.org/10.2760/64633.

Jegan Roy, J., Rarotra, Saptak, Krikstolaityte, Vida, Wu Zhuoran, K., Dja-Ia Cindy, Y., Yi Tan, X., Carboni, Michael, Meyer, Daniel, Yan, Qingyu, Srinivasan, Madhavi, Roy, J. J., Rarotra, S., Krikstolaityte, V., Zhuoran, K.W., d-I Cindy, Y., Yan, Q., Srinivasan, M., Tan, X.Y., Carboni, M., Meyer, D., 2022. Green recycling methods to treat lithium-ion batteries e-waste: a circular approach to sustainability. Adv. Mater. 34, 2103346 https://doi.org/10.1002/ADMA.202103346.

Kang, J., Senanayake, G., Sohn, J., Shin, S.M., 2010. Recovery of cobalt sulfate from spent lithium ion batteries by reductive leaching and solvent extraction with Cyanex 272. Hydrometallurgy 100, 168–171. https://doi.org/10.1016/j.hydromet.2009.10.010.

Kim, J., Paulsen, J., Park, Ar., Kim, D.-H., Gil, H.-S., 2017. Ni based cathode material for rechargeable lithium-ion batteries. EP3428124B1.

Kim, S., Bang, J., Yoo, J., Shin, Y., Bae, J., Jeong, J., Kim, K., Dong, P., Kwon, K., 2021. A comprehensive review on the pretreatment process in lithium-ion battery recycling. J. Clean. Prod. 294 https://doi.org/10.1016/J.JCLEPRO.2021.126329.

Kramer, H.J.M., Lakerveld, R., 2019. Selection and design of industrial crystallizers. In: Erdemir, D., Lee, A.Y., Myerson, A.S. (Eds.), Handbook of Industrial Crystallization. Cambridge University Press, Cambridge, pp. 197–215. https://doi.org/10.1017/9781139026949.007.

Kwade, A., Diekmann, J., 2018. Recycling of Lithium-Ion Batteries. The Lithorec Way, Sustainable Production, Life Cycle Engineering and Management. Springer International Publishing, Cham. https://doi.org/10.1007/978-3-319-70572-9.

Lagnoni, M., Latini, D., Nicolella, C., Tognotti, L., Bertei, A., 2022. Design guidelines for secondary lithium-ion battery electrodes to overcome performance limitations of recycled cathode materials. J. Energy Storage 50, 104237. https://doi.org/10.1016/J.EST.2022.104237.

Lander, L., Cleaver, T., Rajaeifar, M.A., Nguyen-Tien, V., Elliott, R.J.R., Heidrich, O., Kendrick, E., Edge, J.S., Offer, G., 2021. Financial viability of electric vehicle lithium-ion battery recycling. iScience 24. https://doi.org/10.1016/J.ISCI.2021.102787.

Larouche, F., Tedjar, F., Amouzegar, K., Houlachi, G., Bouchard, P., Demopoulos, G.P., Zaghib, K., 2020. Progress and status of hydrometallurgical and direct recycling of Li-Ion batteries and beyond. Materials (Basel). https://doi.org/10.3390/ma13030801.

Latini, D., Vaccari, M., Lagnoni, M., Orefice, M., Mathieux, F., Huisman, J., Tognotti, L., Bertei, A., 2022. A comprehensive review and classification of unit operations with assessment of outputs quality in lithium-ion battery recycling. J. Power Sources 546, 231979. https://doi.org/10.1016/j.jpowsour.2022.231979.

Leal, V.M., Ribeiro, J.S., Coelho, E.L.D., Freitas, M.B.J.G., 2023. Recycling of spent lithium-ion batteries as a sustainable solution to obtain raw materials for different applications. J. Energy Chem. 79, 118–134. https://doi.org/10.1016/j.jechem.2022.08.005.

Lin, J., Zhang, X., Fan, E., Chen, R., Wu, F., Li, L., 2023. Carbon neutrality strategies for sustainable batteries: from structure, recycling, and properties to applications. Energy Environ. Sci. 16, 745–791. https://doi.org/10.1039/D2EE03257K.

Lu, J., Stevens, G.W., Mumford, K.A., 2021. Development of heterogeneous equilibrium model for lithium solvent extraction using organophosphinic acid. Sep. Purif. Technol. 276, 119307 https://doi.org/10.1016/J.SEPPUR.2021.119307.

Maisel, F., Neef, C., Marscheider-Weidemann, F., Nissen, N.F., 2023. A forecast on future raw material demand and recycling potential of lithium-ion batteries in electric vehicles. Resour. Conserv. Recycl. 192, 106920 https://doi.org/10.1016/j.resconrec.2023.106920.

Makuza, B., Tian, Q., Guo, X., Chattopadhyay, K., Yu, D., Huang, Z., Makuza, B., Guo, X., Tian, Q., Guo, X., Chattopadhyay, K., Yu, D., Huang, Z., Makuza, B., Guo, X., Tian, Q., Guo, X., Chattopadhyay, K., Yu, D., 2021. Pyrometallurgical options for recycling spent lithium-ion batteries: a comprehensive review. J. Power Sources. https://doi.org/10.1016/j.jpowsour.2021.229622. Elsevier B.V.

Masias, A., Marcicki, J., Paxton, W.A., 2021. Opportunities and challenges of lithium ion batteries in automotive applications. ACS. Energy Lett. https://doi.org/10.1021/acsenergylett.0c02584.

Meshram, P., Mishra, A., Abhilash, Sahu, R., 2020. Environmental impact of spent lithium ion batteries and green recycling perspectives by organic acids – A review. Chemosphere 242.

Morina, R., Callegari, D., Merli, D., Alberti, G., Mustarelli, P., Quartarone, E., 2022. Cathode active material recycling from spent lithium batteries: a green (circular) approach based on deep eutectic solvents. ChemSusChem. 15 https://doi.org/10.1002/cssc.202102080.

Mossali, E., Picone, N., Gentilini, L., Rodrìguez, O., Pérez, J.M., Colledani, M., 2020. Lithium-ion batteries towards circular economy: a literature review of opportunities and issues of recycling treatments. J. Environ. Manage 264. https://doi.org/10.1016/j.jenvman.2020.110500.

Mrozik, W., Rajaeifar, M.A., Heidrich, O., Christensen, P., 2021. Environmental impacts, pollution sources and pathways of spent lithium-ion batteries. Energy Environ. Sci. 14, 6099–6121. https://doi.org/10.1039/D1EE00691F.

Neumann, J., Petranikova, M., Meeus, M., Gamarra, J.D., Younesi, R., Winter, M., Nowak, S., 2022. Recycling of lithium-ion batteries—current state of the art, circular economy, and next generation recycling. Adv. Energy Mater., 2102917 https://doi.org/10.1002/AENM.202102917.

Or, T., Gourley, S.W.D.D., Kaliyappan, K., Yu, A., Chen, Z., 2020. Recycling of Mixed Cathode Lithium-Ion Batteries For Electric vehicles: Current status and Future outlook, Carbon Energy. Blackwell Publishing Inc. https://doi.org/10.1002/cey2.29.

Punt, F., Doose, S., Böttcher, A., Breitung-Faes, S., Kwade, A., 2023. Modeling and flow sheet simulation of selected mechanical recycling processes for li-ion batteries. Chemie Ingenieur Technik 95, 59–67. https://doi.org/10.1002/cite.202200156.

Qu, G., Wei, Y., Liu, C., Yao, S., Zhou, S., Li, B., 2022. Efficient separation and recovery of lithium through volatilization in the recycling process of spent lithium-ion batteries. Waste Management 150, 66–74. https://doi.org/10.1016/j.wasman.2022.06.039.

Rinne, M., Elomaa, H., Porvali, A., Lundström, M., 2021. Simulation-based life cycle assessment for hydrometallurgical recycling of mixed LIB and NiMH waste. Resour. Conserv. Recycl. 170, 105586 https://doi.org/10.1016/j.resconrec.2021.105586.

Rolland, M., Rakotonirina, A.D., Devouassoux, A., Barrios Goicetty, J.L., Delenne, J.Y., Wachs, A., 2019. Predicting average void fraction and void fraction uncertainty in fixed beds of poly lobed particles. Ind. Eng. Chem. Res. 58, 3902–3911. https://doi.org/10.1021/acs.iecr.8b05557.

Sommerville, R., Zhu, P., Rajaeifar, M.A., Heidrich, O., Goodship, V., Kendrick, E., 2021. A qualitative assessment of lithium ion battery recycling processes. Resour. Conserv. Recycl. 165 https://doi.org/10.1016/j.resconrec.2020.105219.

Sonoc, A., Jeswiet, J., Soo, V.K., 2015. Opportunities to improve recycling of automotive lithium ion batteries. Procedia CIRP. Elsevier B.V., pp. 752–757. https://doi.org/10.1016/j.procir.2015.02.039

Tao, Y., Wang, Z., Wu, B., Tang, Y., Evans, S., 2023. Environmental life cycle assessment of recycling technologies for ternary lithium-ion batteries. J. Clean. Prod. 389, 136008 https://doi.org/10.1016/j.jclepro.2023.136008.

Thompson, D., Hyde, C., Hartley, J.M., Abbott, A.P., Anderson, P.A., Harper, G.D.J., 2021. To shred or not to shred: a comparative techno-economic assessment of lithium ion battery hydrometallurgical recycling retaining value and improving circularity in LIB supply chains. Resour. Conserv. Recycl. 175, 105741 https://doi.org/10.1016/J.RESCONREC.2021.105741.

Thompson, D.L., Hartley, J.M., Lambert, S.M., Shiref, M., Harper, G.D.J., Kendrick, E., Anderson, P., Ryder, K.S., Gaines, L., Abbott, A.P., 2020. The importance of design in lithium ion battery recycling-a critical review. Green Chem. https://doi.org/10.1039/D0GC02745F.

Vaccari, M., Barontini, F., Bertei, A., Puccini, M., Tognotti, L., 2023. Co-precipitation of cathode active materials precursors in lithium-ion batteries recycling: experiments and modeling. Chem. Eng. Trans. 99, 169–174. https://doi.org/10.3303/CET2399029.

Vassart, A., 2013. EBRA guidance document on the calculation of recycling efficiencies for spent batteries and accumulators.

Wang, Y., Xu, Z., Zhang, X., Sun, M., Tu, Y., 2023. Separation of Cu impurity from spent lithium-ion batteries by roasting in air and leaching with (NH4)2CO3 solution of low concentration. Hydrometallurgy 216, 106000. https://doi.org/10.1016/j.hydromet.2022.106000.

Wasesa, M., Hidayat, T., Andariesta, D.T., Natha, M.G., Attazahri, A.K., Afrianto, M.A., Mubarok, M.Z., Zulhan, Z., Putro, U.S., 2022. Economic and environmental assessments of an integrated lithium-ion battery waste recycling supply chain: a hybrid simulation approach. J. Clean. Prod. 379, 134625 https://doi.org/10.1016/J.JCLEPRO.2022.134625.

Windisch-Kern, S., Gerold, E., Nigl, T., Jandric, A., Altendorfer, M., Rutrecht, B., Scherhaufer, S., Raupenstrauch, H., Pomberger, R., Antrekowitsch, H., Part, F., 2022. Recycling chains for lithium-ion batteries: a critical examination of current challenges, opportunities and process dependencies. Waste Manage. Pergamon. https://doi.org/10.1016/J.WASMAN.2021.11.038.

Wu, J., Zheng, M., Liu, T., Wang, Y., Liu, Y., Nai, J., Zhang, L., Zhang, S., Tao, X., 2023. Direct recovery: a sustainable recycling technology for spent lithium-ion battery. Energy Storage Mater. 54, 120–134. https://doi.org/10.1016/j.ensm.2022.09.029.

Xu, P., Dai, Q., Gao, H., Liu, H., Zhang, M., Li, M., Chen, Y., An, K., Meng, Y.S., Liu, P., Li, Y., Spangenberger, J.S., Gaines, L., Lu, J., Chen, Z., 2020. Efficient direct recycling of lithium-ion battery cathodes by targeted healing. Joule 4, 2609–2626. https://doi.org/10.1016/j.joule.2020.10.008.

Yang, T., Luo, D., Yu, A., Chen, Z., 2023. Enabling future closed-loop recycling of spent lithium-ion batteries: direct cathode regeneration. Adv. Materi. 35 https://doi.org/10.1002/adma.202203218.

Yang, Y., Okonkwo, E.G., Huang, G., Xu, S., Sun, W., He, Y., 2021. On the Sustainability of Lithium Ion Battery Industry – A review and perspective, Energy Storage Materials. Elsevier B.V. https://doi.org/10.1016/j.ensm.2020.12.019.

Yu, M., Bai, B., Xiong, S., Liao, X., 2021. Evaluating environmental impacts and economic performance of remanufacturing electric vehicle lithium-ion batteries. J. Clean. Prod. 321, 128935 https://doi.org/10.1016/j.jclepro.2021.128935.

Yuan, G., Liu, X., Zhang, C., Pham, D.T., Li, Z., 2023. A new heuristic algorithm based on multi-criteria resilience assessment of human–robot collaboration disassembly for supporting spent lithium-ion battery recycling. Eng. Appl. Artif. Intell. 126, 106878 https://doi.org/10.1016/J.ENGAPPAI.2023.106878.

Zhang, B., Xu, Y., Makuza, B., Zhu, F., Wang, H., Hong, N., Long, Z., Deng, W., Zou, G., Hou, H., Ji, X., 2023. Selective lithium extraction and regeneration of LiCoO2 cathode materials from the spent lithium-ion battery. Chem. Eng. J. 452, 139258 https://doi.org/10.1016/j.cej.2022.139258.

Zhang, J., Hu, J., Zhang, W., Chen, Y., Wang, C., 2018. Efficient and economical recovery of lithium, cobalt, nickel, manganese from cathode scrap of spent lithium-ion batteries. J. Clean. Prod. 204, 437–446. https://doi.org/10.1016/j.jclepro.2018.09.033.

SUPPLEMENTARY INFORMATION

Assessing performance in Lithium-ion batteries recycling processes: a quantitative modelling perspective

Marco Vaccari[1]*, Filippo Parlanti[1], Fabio M. Manni[2], Martina Orefice[2], Fabrice Mathieux[2], Gabriele Pannocchia[1], Leonardo Tognotti[1], Antonio Bertei[1]*

[1]Department of Civil and Industrial Engineering, University of Pisa, Largo Lazzarino 2, 56122 Pisa, Italy

[2]European Commission – Joint Research Centre, Sustainable Resources Directorate, Via E. Fermi 2749, 21027 Ispra, Italy

**marco.vaccari@unipi.it, antonio.bertei@unipi.it*

S1. Process modeling details

With reference to Figure 2 of the paper we here list the modeling details used to simulate the two processes.

S1.1. Umicore-Valéas Process

The leaching reactions involved and modeled for the unit operation "*Leaching*" are reported in Eq. (S1).

$$\begin{aligned} Fe + 1.5\,H_2SO_4 &\leftrightarrow 0.5\,Fe_2(SO_4)_3 + 1.5\,H_2 \\ Cu + H_2SO_4 &\leftrightarrow CuSO_4 + H_2 \\ Ni + H_2SO_4 &\leftrightarrow NiSO_4 + H_2 \\ Co + H_2SO_4 &\leftrightarrow CoSO_4 + H_2 \end{aligned} \tag{S1}$$

The power consumption of the impellers in stirred reactors is calculated by using the power number (Np) definition for impellers (Green and Southard, 2019) in Eq (S2).

$$P\,[kW] = Np \cdot \rho \cdot N^3 \cdot D^5 \tag{S2}$$

with ρ calculated in the code as suspension density [kg/m^3], N as operative mixing speed [rpm] fixed to be twice the just suspended mixing speed, and D [m] as the impeller diameter. Np refers to a Propeller A-310 in turbulent conditions and is taken from the literature (Post Mixing, 2013).

S2.2. LithoRec Process

In all hydrometallurgical unit operations liquid solutions are supposed to be ideal, hence summing the volume of two or more different solutions is equal to the volume of the resulting mix of solutions. In addition, the effects of solid compounds and of chemical reactions on solution volume is supposed to be negligible.

Modeling of the leaching equilibria for the LFP and the reactions considered in the model of this operation, the acid/base equilibria of phosphates ions are reported in equation (S3).

$$\begin{aligned} H_3PO_4 + H_2O &\leftrightarrow H_2PO_4^- + H_3O^+ && \text{pK1} = 2.15 \\ H_2PO_4^- + H_2O &\leftrightarrow HPO_4^{2-} + H_3O^+ && \text{pK2} = 7.20 \\ HPO_4^{2-} + H_2O &\leftrightarrow PO_4^{3-} + H_3O^+ && \text{pK3} = 12.38 \end{aligned} \tag{S3}$$

Thus, when pH is much higher than pK1, that is in the impurities removal step, all the H_3PO_4 is turned into $H_2PO_4^-$ and its effect has to be neutralized by adding NaOH solution. When pH is much higher than pK2, that is in the co-precipitation step, all the $H_2PO_4^-$ is turned into HPO_4^{2-} and its effect has to be neutralized adding more NaOH solution.

Table S1. *Parameters adopted to simulate the pyrometallurgy-based route.*

PYRO LIBs RECYCLING				
Unit operation	**Parameters**	**Values**		**Source**
Disassembly	Fractions of input materials that goes to the manual sorting step (kg/kg)	Electr&Cables	1	Elaborated from: [1,2]
		Fe	0.84	
		Plastics	0.32	
		Al	0.926	
Manual Sorting	Fractions of input materials that goes into the more valuable fractions stream (kg/kg)	Electr&Cables	0.3939	Elaborated from: [1,2]
		Fe	0.2393	
		Plastics	0.0523	
		Al	0.7537	
Smelting	Fractions of input materials that goes into the alloy (kg/kg)	Fe	0.645	[3]
		Cu	0.928	
		Co	0.940	
		Ni	0.990	
	Addition ratio - mass to be fed for 1 kg of input into the smelter (kg/kg)	Al2O3	0.018	
		C	0.333	
		CaO	0.067	
		CaCO3	0.083	
		SiO2	0.148	
		Others	0.025	
	Air flow ratio (m^3/kg)	9.5		From post-process calculation
	Average heat requirement for a ton of materials in input (MJ/tons)	5000		[4]
	Air Temperature (°C)	500		[3]
	Smelter Pressure (atm)	1		
	O_2 in air (mol/mol)	0.4		
Alloy Crushing	Dp (mm)	100		**Hypothesis**
Leaching	Leaching efficiency - amount of leached metal in the solution divided by the total amount of that metal present in the black mass (mol/mol)	Fe	0.99	**Conservative hypothesis**
		Cu	0.99	
		Ni	0.98	[5]
		Co	0.96	
	Concentration H_2SO_4 (M)	5.43		
	H_2SO_4 input excess (mol/mol)	0.15		
	pH	2 < pH < 2.5		
	T (°C)	55		
Washing of leaching filter cake	Humidity (kg/kg)	0.099		Elaborated from: [6]
	Ratio (r) between the washing solution and the humidity of the filter cake (kg/kg)	2		**Hypothesis** †
Cu precipitation	Precipitation efficiency - Cu removed from the solution divided by Cu in the initial solution (kg/kg)	0.99		[7]
	SO_2 vol frac in/out	0.98	0.90	**Supposed** in order to minimize the gas flow
	T (°C)	60		
	P (atm)	3		
Washing of CuS filter cake	Humidity (kg/kg)	0.240		Elaborated from [6]
	Liquid to solid ratio r (kg/kg)	2		**Hypothesis** †
Fe precipitation	pH	6 (to be in the range 4.5-6)		From calculation and equilibrium data

	Concentration NaOH (M)	5	**Hypothesis**
Washing of Fe filter cake	Humidity (kg/kg)	0.226	Elaborated from [6]
	Liquid to solid ratio r (kg/kg)	2	**Hypothesis** †
Co extraction	Extractant concentration (M)	0.4	[8]
	Ratio between Org. solvent and Aq. Solution (m^3/m^3)	3	
	Saponified extractant fraction (mol/mol)	0.5	
	Ratio between Cu extracted in the organic phase and Cu left in the aqueous phase (mol/mol)	0.99	Elaborated from: [9]
	Co and Ni extraction efficiencies (mol/mol)	f (pH, saponified extractant fraction)	
Organic phase stripping	pH	2.5	[10]
	NaOH input excess (mol/mol)	0.05	
Ni precipitation	pH	11	From calculation and equilibrium data
Washing of Ni filter cake	Humidity (kg/kg)	0.112	Elaborated from [6]
	Liquid to solid ratio r (kg/kg)	2	**Hypothesis** †
CoCl2 crystallization	T concentrator (°C)	60	From design sizing
	T crystallizator (°C)	30	
	C concentrator out (g/g solvent)	0.58	
	Humidity of crystal (kg/kg)	0.1	
Washing of Co filter cake	Liquid to solid ratio r (kg/kg)	2	**Hypothesis** †
Drying	Temperature (°C)	75	**Hypothesis**
	Fraction of water removed from the wet solid (kg/kg)	0.98	
	Overall heating method efficiency	0.3	
Wastewater neutralization	H_2SO_4 input/wastewater (m^3/m^3)	0.00064	From post-process calculation

Table S2. *Parameters adopted to simulate the hydrometallurgy-based route.*

HYDRO LIBs RECYCLING				
Unit operation	**Parameters**	**Values**		**Source**
Disassembly	Fractions of input materials that goes to the manual sorting step (kg/kg)	Electr&Cables	1	Elaborated from: [1,2]
		Fe	0.84	
		Plastics	0.32	
		Al	0.926	
Manual Sorting	Fractions of input materials that goes into the more valuable fractions stream (kg/kg)	Electr&Cables	0.3939	Elaborated from: [1,2]
		Fe	0.2393	
		Plastics	0.0523	
		Al	0.7537	
Inert crushing	Overall electrolyte loss (kg/kg)	0.045		[2]
	Auxiliary mass ratio for re-integration in the recirculating wet scrubber (kg/kg)	N2	0.01377	From design sizing
		NaOH	$6.64 \cdot 10^{-4}$	
		H2O	$3.15 \cdot 10^{-3}$	
	Share of electrolyte solvents in off gas (kg/kg)	EC	0.0247	[2]
		CHB	0.3260	
		DMC	0.0423	
		EMC	0.0645	
Electrolyte Extraction with sub-critical CO2	Overall extraction efficiency (kg/kg)	0.891		[11]
	Polar compound extraction efficiency (kg/kg)	0.92		[11]
	Mass ratio cosolvent/flow to electrolyte extraction (kg/kg)	0.4451		From design sizing
	ACN fraction in co-solvent (mol/mol)	0.75		[11]
	Mass ratio CO_2 recirculated/flow to electrolyte extraction (kg/h)/(kg/h)	4.887		From design sizing
	Ratio CO_2 fresh/CO_2 recirculated (kg/kg)	0.0348		From rigorous simulation
Air Classification 1	Fractions of any compound in the incoming stream that is separated in the heavy fraction (kg/kg)	Fe	0.9569	Elaborated from: [1,2] + **hypothesis** that inclusions in the first heavy fraction have the same composition as the material input.
		Plastics	0.0508	
		Al	0.5725	
		Cu	0.0591	
		C, Li, Co, Mn, Ni, P, O, Si, PVDF	0.0051	
Magnetic Separation	Fractions of any compound in input that is separated in the magnetic fraction (kg/kg)	Fe	0.98	**Hypothesis**
		Plastics	0.01	
		Al	0.01	
		Cu	0.01	
		C, Li, Co, Mn, Ni, P, O, Si, PVDF	0.01	
Sieving	Fractions of the component that ends up in the black mass (kg/kg)	Fe	0.9772	Elaborated from: [1,2]
		Al	0.0291	
		Cu	0.0444	

		C, Li, Co, Mn, Ni, P, O, Si, PVDF	0.8569	
Air Classification 2	Fraction that goes into the heavy fraction (kg/kg)	Fe	1	Elaborated from: [1,2]
		Plastics	0.638	
		Al	0.991	
		Cu	1	
		C, Li, Co, Mn, Ni, P, O, Si, PVDF	1	
Optical Separation 1	Al content in accepted output (kg/kg)	0.931		[12]
	Al content in rejected output (kg/kg)	0.025		
Optical Separation 2	Al content in accepted output (kg/kg)	0.003		
	Al content in rejected output (kg/kg)	0.782		
Leaching	Leaching efficiency - amount of leached metal in the solution divided by the total amount of that metal present in the black mass (mol/mol)	Li	0.96	**Conservative hypothesis**
		Ni	0.99	[13]
		Mn	0.96	
		Co	0.96	
		Fe	0.99	**Conservative hypothesis**
		Al	0.99	
		Cu	0.99	
		P	0.99	
	Concentration H_2SO_4 (M)	4		[13]
	Concentration H_2O_2 (wt%)	0.5		
	H_2SO_4 input excess (mol/mol)	0.383		
	H_2O_2 input excess (mol/mol)	11.43		
	pH	1 < pH < 3		
Washing of leaching filter cake	Humidity (kg/kg)	0.163		Elaborated from [6])
	Ratio (r) between the washing solution and the humidity of the filter cake (kg/kg)	2		**Hypothesis** †
Drying of graphite	Fraction of water removed from the wet solid (kg/kg)	0.98		**Hypothesis** ◆
Impurities removal	pH	6.47		[14]
	T (°C)	60		
Washing of impurities filter cake	Humidity (kg/kg)	0.229		Elaborated from [6])
	Liquid to solid ratio r (kg/kg)	2		**Hypothesis** †
Drying of impurities	Fraction of water removed from the wet solid (kg/kg)	0.98		**Hypothesis** ◆
Co-precipitation	Concentration NH_3 solution (M)	5		[15]
	Concentration NH_3 bulk (M)	1		
	Solubility NMC (M)	0.1		[16]
	Vvm (m^3/(min·m^3)): volumetric flow of nitrogen bubbled in the stirred tank divided by the total volume of solution in the stirred tank	$7.57 \cdot 10^{-5}$		Van Bommet et al.,2009
Washing of co-precipitation filter cake	Humidity (kg/kg)	0.178		Elaborated from [6])
	Liquid to solid ratio r (kg/kg)	2		**Hypothesis** †
Drying of precursor	Fraction of water removed from the wet solid (kg/kg)	0.98		**Hypothesis** ◆
Li recovery	Yield prec. (mol/mol): flow of Li precipitated as Li_2CO_3 divided by the total amount of Li in the solution before the Li recovery step	0.75		[17]
	Solubility Na_2CO_3 (M)	4.4811		
Washing of Li2CO3	Humidity (kg/kg)	0.305		Elaborated from [6])
	Liquid to solid ratio r (kg/kg)	2		**Hypothesis** †
Drying of Li2CO3	Fraction of water removed from the wet solid (kg/kg)	0,98		**Hypothesis** ◆
	Heat exchanger efficiency (kWh/kWh)	0.75		
Sintering	Air molar ratio = O_2 molar ratio: molar ratio between air (or O_2) incoming the furnace and air (or O_2) reacted	4		**Hypothesis** (typical value for enriched air)
	Li_2CO_3 input excess (mol/mol)	0.085:0.1 (depends on which cathode is re-sintered)		[18,19])

	Furnace energy efficiency (kWh/kWh)	0.8	**Hypothesis**
Heating	Absolute humidity (kg/kg)	0.009	**Hypothesis**
	Energy eff. Boiler (kWh/kWh)	0.75	

Table S3. *Mass composition adopted in the code for different LIB chemistries and formats.*

LIBs part	Material	LARGE						SMALL							
		NMC 111	NMC 532	NMC 622	NMC 811	NCA	LFP	NMC 111	NMC 532	NMC 622	NMC 811	NCA	LFP	LCO	LMO
Pack	Steel	5.7%	5.7%	5.7%	5.7%	5.7%	5.7%	0.0%	0.0%	0.0%	0.0%	0.0%	0.0%	0.0%	0.0%
	Electr. and Cables	5.0%	5.0%	5.0%	5.0%	5.0%	5.0%	0.0%	0.0%	0.0%	0.0%	0.0%	0.0%	0.0%	0.0%
	Al	18.0%	18.0%	18.0%	18.0%	18.0%	18.0%	0.0%	0.0%	0.0%	0.0%	0.0%	0.0%	0.0%	0.0%
	Plastics	5.7%	5.7%	5.7%	5.7%	5.7%	5.7%	0.0%	0.0%	0.0%	0.0%	0.0%	0.0%	0.0%	0.0%
Module	Al	5.2%	5.2%	5.2%	5.2%	5.2%	5.2%	0.0%	0.0%	0.0%	0.0%	0.0%	0.0%	0.0%	0.0%
	Plastics	1.5%	1.5%	1.5%	1.5%	1.5%	1.5%	0.0%	0.0%	0.0%	0.0%	0.0%	0.0%	0.0%	0.0%
	Steel	3.3%	3.3%	3.3%	3.3%	3.3%	3.3%	0.0%	0.0%	0.0%	0.0%	0.0%	0.0%	0.0%	0.0%
Casing	Al	6.9%	6.8%	6.9%	6.8%	6.8%	5.4%	0.0%	0.0%	0.0%	0.0%	0.0%	0.0%	0.0%	0.0%
	Steel	0.0%	0.0%	0.0%	0.0%	0.0%	0.0%	13.9%	14.0%	14.1%	14.2%	14.1%	14.4%	15.9%	13.5%
Cell	Al foil	4.5%	5.4%	5.7%	6.0%	5.6%	7.4%	9.3%	8.9%	8.8%	8.6%	8.8%	11.1%	10.6%	9.8%
	Cu foil	7.5%	8.9%	9.4%	9.9%	9.3%	12.1%	15.3%	14.8%	14.5%	14.3%	14.6%	18.4%	17.5%	16.2%
	Graphite	7.6%	7.6%	7.6%	7.6%	7.6%	5.2%	12.6%	13.7%	14.3%	14.8%	14.2%	9.4%	14.6%	10.4%
	Li	1.2%	1.1%	1.0%	1.0%	1.0%	0.5%	2.0%	1.9%	1.9%	1.9%	1.9%	1.0%	1.2%	1.2%
	Co	3.4%	1.8%	1.7%	0.8%	1.3%	0.0%	5.6%	3.3%	3.2%	1.6%	2.4%	0.0%	10.1%	0.0%
	Mn	3.2%	2.5%	1.6%	0.8%	0.0%	0.0%	5.2%	4.6%	3.0%	1.5%	0.0%	0.0%	0.0%	18.6%
	Ni	3.4%	4.5%	5.1%	6.4%	6.8%	0.0%	5.6%	8.2%	9.6%	12.6%	12.8%	0.0%	0.0%	0.0%
	Al	0.0%	0.0%	0.0%	0.0%	0.2%	0.0%	0.0%	0.0%	0.0%	0.0%	0.4%	0.0%	0.0%	0.0%
	Fe	0.0%	0.0%	0.0%	0.0%	0.0%	4.3%	0.0%	0.0%	0.0%	0.0%	0.0%	8.1%	0.0%	0.0%
	P	0.0%	0.0%	0.0%	0.0%	0.0%	2.4%	0.0%	0.0%	0.0%	0.0%	0.0%	4.5%	0.0%	0.0%
	O	5.5%	4.9%	4.6%	4.4%	4.7%	4.9%	9.2%	8.9%	8.7%	8.6%	8.7%	9.3%	5.5%	10.8%
	PP	1.0%	1.2%	1.3%	1.4%	1.3%	1.7%	2.1%	2.0%	2.0%	2.0%	2.0%	2.6%	2.4%	2.2%
	PVDF	1.3%	1.2%	1.2%	1.2%	2.0%	2.2%	2.1%	2.2%	2.3%	2.3%	2.4%	4.1%	2.5%	1.1%
	EC	2.6%	2.5%	2.5%	2.5%	2.3%	2.3%	4.4%	4.5%	4.5%	4.6%	4.5%	4.1%	5.0%	4.0%
	CHB	0.1%	0.1%	0.1%	0.1%	0.1%	0.1%	0.1%	0.1%	0.2%	0.1%	0.1%	0.1%	0.2%	0.1%
	DMC	3.0%	2.9%	2.9%	2.9%	2.7%	2.7%	5.1%	5.2%	5.3%	5.5%	5.3%	4.8%	5.9%	4.7%
	EMC	1.9%	1.8%	1.8%	1.8%	1.7%	1.7%	3.2%	3.3%	3.3%	3.3%	3.3%	3.0%	3.7%	2.9%
	LiPF6	1.0%	1.0%	1.0%	1.0%	0.9%	0.9%	1.7%	1.8%	1.8%	1.8%	1.8%	1.6%	2.0%	1.6%
	CB	1.5%	1.4%	1.2%	1.1%	1.3%	1.8%	2.6%	2.6%	2.5%	2.3%	2.7%	3.1%	2.9%	2.7%

References

[1] A. Kwade, J. Diekmann, Recycling of Lithium-Ion Batteries. The LithoRec Way, Springer International Publishing, Cham, 2018. https://doi.org/10.1007/978-3-319-70572-9.

[2] J. Diekmann, C. Hanisch, L. Froböse, G. Schälicke, T. Loellhoeffel, A.-S. Fölster, A. Kwade, Ecological Recycling of Lithium-Ion Batteries from Electric Vehicles with Focus on Mechanical Processes, J Electrochem Soc. 164 (2017) A6184–A6191. https://doi.org/10.1149/2.0271701JES.

[3] D. Cheret, S. Santen, Battery Recycling. US 7169206 B2, (2007).

[4] A. Sonoc, J. Jeswiet, V.K. Soo, Opportunities to improve recycling of automotive lithium ion batteries, in: Procedia CIRP, Elsevier B.V., 2015: pp. 752–757. https://doi.org/10.1016/j.procir.2015.02.039.

[5] J. Zhang, J. Hu, W. Zhang, Y. Chen, C. Wang, Efficient and economical recovery of lithium, cobalt, nickel, manganese from cathode scrap of spent lithium-ion batteries, J Clean Prod. 204 (2018) 437–446. https://doi.org/10.1016/j.jclepro.2018.09.033.

[6] M. Rolland, A.D. Rakotonirina, A. Devouassoux, J.L. Barrios Goicetty, J.Y. Delenne, A. Wachs, Predicting Average Void Fraction and Void Fraction Uncertainty in Fixed Beds of Poly Lobed Particles, Ind Eng Chem Res. 58 (2019) 3902–3911. https://doi.org/10.1021/ACS.IECR.8B05557/ASSET/IMAGES/LARGE/IE-2018-05557P_0011.JPEG.

[7] H. Estay, L. Barros, E. Troncoso, Metal Sulfide Precipitation: Recent Breakthroughs and Future Outlooks, Minerals 2021, Vol. 11, Page 1385. 11 (2021) 1385. https://doi.org/10.3390/MIN11121385.

[8] J. Kang, G. Senanayake, J. Sohn, S.M. Shin, Recovery of cobalt sulfate from spent lithium ion batteries by reductive leaching and solvent extraction with Cyanex 272, Hydrometallurgy. 100 (2010) 168–171. https://doi.org/10.1016/j.hydromet.2009.10.010.

[9] V.N.H. Nguyen, T.H. Nguyen, M.S. Lee, Review on the Comparison of the Chemical Reactivity of Cyanex 272, Cyanex 301 and Cyanex 302 for Their Application to Metal Separation from Acid Media, Metals 2020, Vol. 10, Page 1105. 10 (2020) 1105. https://doi.org/10.3390/MET10081105.

[10] D.S. Flett, Solvent extraction in hydrometallurgy: the role of organophosphorus extractants, J Organomet Chem. 690 (2005) 2426–2438. https://doi.org/10.1016/J.JORGANCHEM.2004.11.037.

[11] M. Grützke, X. Mönnighoff, F. Horsthemke, V. Kraft, M. Winter, S. Nowak, Extraction of lithium-ion battery electrolytes with liquid and supercritical carbon dioxide and additional solvents, RSC Adv. 5 (2015) 43209–43217. https://doi.org/10.1039/c5ra04451k.

[12] C. Mämpel, Recycling von Lithium-Ionen-Batterien aus Elektromobilen, Technische Universität Bergakademie Freiberg, 2013.

[13] E. Gratz, Q. Sa, D. Apelian, Y. Wang, A closed loop process for recycling spent lithium ion batteries, J Power Sources. 262 (2014) 255–262. https://doi.org/10.1016/j.jpowsour.2014.03.126.

[14] T. Or, S.W.D.D. Gourley, K. Kaliyappan, A. Yu, Z. Chen, Recycling of mixed cathode lithium-ion batteries for electric vehicles: Current status and future outlook, Carbon Energy. 2 (2020) 6–43. https://doi.org/10.1002/cey2.29.

[15] P. Barai, Z. Feng, H. Kondo, V. Srinivasan, Multiscale Computational Model for Particle Size Evolution during Coprecipitation of Li-Ion Battery Cathode Precursors, J Phys Chem B. 123 (2019) 3291–3303. https://doi.org/10.1021/acs.jpcb.8b12004.

[16] G. Giovannetti, M. Guagnano, Studio di processi di recupero di materiali catodici da batterie litio-ione esauste, University of Pisa, 2022.

[17] B. Han, R. Anwar UI Haq, M. Louhi-Kultanen, Lithium carbonate precipitation by homogeneous and heterogeneous reactive crystallization, Hydrometallurgy. 195 (2020) 105386. https://doi.org/10.1016/j.hydromet.2020.105386.

[18] J. Kim, J. PAULSEN, Ar. PARK, D.-H. KIM, H.-S. GIL, NI BASED CATHODE MATERIAL FOR RECHARGEABLE LITHIUM-ION BATTERIES, EP3428124B1, 2017.

[19] J. Paulsen, D. Nelis, J. Hu, L. Zhu, E. Robert, Precursors for cathode material with improved secondary battery performance and method to prepare the precursors, US11476461B2, 2017.